






RESEARCH ARTICLE | JANUARY 02 2025

Aerodynamics of two rough circular cylinders placed side by side subject to postcritical flow

Anil Pasam ; Daniel Tudball Smith ; David Burton ; Mark C. Thompson  



Physics of Fluids 37, 015105 (2025)

<https://doi.org/10.1063/5.0241365>



Articles You May Be Interested In

Flow over two inline rough cylinders in the postcritical regime

Physics of Fluids (September 2024)

Systematical study on the aerodynamic control mechanisms of a 1:2 rectangular cylinder with Kirigami scales

Physics of Fluids (July 2024)

Influence of inertia and gravity on the stability of filament jet flow

Physics of Fluids (June 2006)



Physics of Fluids

Special Topics Open
for Submissions

[Learn More](#)



Aerodynamics of two rough circular cylinders placed side by side subject to postcritical flow

Cite as: Phys. Fluids **37**, 015105 (2025); doi: [10.1063/5.0241365](https://doi.org/10.1063/5.0241365)
 Submitted: 30 September 2024 · Accepted: 2 December 2024 ·
 Published Online: 2 January 2025



View Online



Export Citation



CrossMark

Anil Pasam, Daniel Tudball Smith, David Burton, and Mark C. Thompson^{a)}

AFFILIATIONS

Fluids Laboratory for Aeronautical and Industrial Research (FLAIR), Department of Mechanical and Aerospace Engineering, Monash University, Clayton, VIC 3800, Australia

^{a)} Author to whom correspondence should be addressed: mark.thompson@monash.edu

ABSTRACT

This investigation reports on the flow behavior of, and the resulting forces on, two roughened cylinders in the postcritical regime. Specifically, two cylinders of the same surface roughness of $k_s/D = 1.9 \times 10^{-3}$, placed apart at a cross-stream pitch (separation) of $1.18 \leq L/D \leq 6$, are studied at a postcritical Reynolds number of 3×10^5 using unsteady pressure measurements. The two cylinders behave nearly independently at $L/D = 6$ and the forces on them are the same within experimental uncertainty until the pitch ratio is reduced to $L/D = 2.25$. The gap flow between the two cylinders becomes biased at $L/D \leq 2$, with the bias well correlated across the span for $1.33 \leq L/D \leq 2$. In addition to the conventional narrow-wake (NW) and wide-wake (WW) modes observed at subcritical Reynolds numbers, a less-biased intermittent gap flow is observed for $L/D = \{1.18, 1.2\}$. Intermittency is observed for some spanwise cross sections, thus reducing the spanwise coherence of the flow. Across pitch ratios investigated, the average of drag coefficients for the two cylinders was always larger than for a single cylinder. For $L/D = \{1.33, 1.5, 1.75\}$, the cylinder with the larger drag experiences a larger lift. Both of these observations are contrary to previous findings in subcritical flows. On the cylinder halves facing the gap, the boundary layer on the cylinder in the NW mode separates further downstream than for the WW mode. This NW separation angle decreases with increasing pitch ratio while it remains similar for the WW mode across pitch ratios.

© 2025 Author(s). All article content, except where otherwise noted, is licensed under a Creative Commons Attribution (CC BY) license (<https://creativecommons.org/licenses/by/4.0/>). <https://doi.org/10.1063/5.0241365>

I. INTRODUCTION

Circular cylinders commonly form critical building blocks of engineered structures. Often, cylinders are situated in close proximity to each other, thus resulting in aerodynamic interactions between them when subject to atmospheric flows. Under extreme wind conditions, the induced aerodynamic forces and moments can be substantial. Hence it is important to quantify these to design structures that are structurally sound.

The current work studies a common baseline arrangement, two cylinders placed beside each other with no streamwise separation. To date, it appears that there are a few studies examining this arrangement in the postcritical flow regime that is relevant to many large engineered structures.

Based on the variation of the drag coefficient with increasing Reynolds number, flow over an isolated cylinder can be classified into four regimes: subcritical, critical, supercritical, and trans/postcritical (Roshko, 1961). Here, the Reynolds number is defined as $Re = \rho U_\infty D / \mu$, where D , μ , U_∞ and ρ are the (same) diameter of the two cylinders, the dynamic viscosity, the velocity, and the density of

the incoming flow, respectively. In the postcritical regime, the transition to turbulence in the cylinder boundary layer occurs sufficiently far upstream of flow separation that any further increase in the Reynolds number has a relatively minor influence on the flow behavior.

For smooth cylinders, the Reynolds number range pertaining to the postcritical flow is $Re > \mathcal{O}(5 \times 10^5)$ (Schewe, 1983). An increase in surface roughness of the cylinder reduces the critical Reynolds number (Achenbach, 1971). Owing to large diameters and a non-negligible surface roughness caused by non-uniform paint, rust, etc., large engineered structures, such as oil/gas rig flare towers or chimney stacks often encounter postcritical flows. For example, for 1 m diameter (D) cylinders in $U_\infty = 100$ m/s (extreme) cyclonic conditions, the Reynolds number is $Re = \mathcal{O}(10^7)$.

This Reynolds number regime has received little attention previously primarily due to large wind tunnel test sections needed to maintain acceptable blockage ratios while using cylinders of large diameters. The current study investigates this particular flow scenario, i.e., *post-critical flow over two rough cylinders placed side-by-side*.

Zdravkovich (1977), Sumner (2010), and Zhou and Alam (2016) reviewed the experimental work involving flow over two smooth cylinders in various arrangements and Reynolds numbers. The presence of another cylinder in the vicinity causes a significant change in flow characteristics relative to those for a single cylinder. For a fixed Reynolds number, the flow behavior is largely governed by the distance between the cylinders. For the remainder of this paper, this is represented by the non-dimensional pitch ratio $L^* = L/D$, where L is the distance between the centers of the two cylinders and D is the cylinder diameter.

For subcritical smooth cylinder flows, three different flow regimes have been previously identified based on the vortex shedding and the behavior of the flow through the gap, these regimes are illustrated in Fig. 1 and are described as follows.

- (i) The *single bluff body regime* where the two cylinders behave similarly to a single body subject to base bleed. The bleed flow increases the formation length of the cylinders, thereby decreasing the drag experienced by the cylinders. This regime exists over $L^* < 1.1 - 1.2$ (Sumner, 2010). For $L^* \leq 1.13$ and for an incoming Reynolds number of 4.7×10^4 , Alam and Zhou (2007) found that the gap flow forms a highly intermittent separation bubble on one of the cylinders, thus resulting in multiple stable flow configurations at the same pitch ratio.
- (ii) The *biased flow regime* where the gap flow is biased toward one of the cylinders and away from the centerline as illustrated in Fig. 1(b). This bias is known to be bi-stable, with the deflection alternating toward either cylinder. The vortex street toward which the gap flow is biased is said to be in the “narrow-wake” mode (NW), while the other vortex street is in the “wide-wake” mode (WW). The biased flow regime is also known to lead to a far wake with two distinct frequencies, with the higher frequency originating from the narrow-wake side (Williamson, 1985). This regime exists over $1.2 < L^* < 2.2$. In addition, Alam et al. (2003) identified $2.2 < L^* < 2.5$ as transitional pitch ratios where the near wake is partly deflected, but only a single prominent frequency is found in the wake.

- (iii) The *parallel vortex streets regime* (PVS) where both cylinders shed vortices into separate wake streets. However, synchronization of vortex shedding exists between the cylinders and the shedding is found to be predominantly out-of-phase (Williamson, 1985; Alam et al., 2003). This regime is seen with pitch ratios in the range $L^* \geq 2 - 2.2$ (Sumner, 2010).

The pitch ratios at which these flow configurations exist, i.e., the boundaries of each regime, vary only slightly depending on the Reynolds number and the experimental setup (Sumner, 2010).

Williamson (1985) studied the wake behind the two cylinders and identified the modes of vortex amalgamation at low Reynolds numbers ($Re \leq 200$). Zhou et al. (2002) investigated velocity distributions up to 40 diameters downstream of the two cylinders to identify the interactions between the rows of vortices at $L^* = \{1.5, 3\}$ for $Re = 5800$. Strouhal numbers in the wake were identified by Bearman and Wadcock (1973), Spivack (1946), and Alam et al. (2003), among others. The influence of Reynolds number on the wake pattern and the frequencies in it, behind this arrangement is relatively small when compared to the one where one cylinder is directly downstream of the other (Xu et al., 2003).

Despite numerous investigations studying the flow behavior in the near and far wakes of the two cylinder arrangement, the mean and fluctuating aerodynamic forces and pressure distributions have been less explored even in the subcritical regime (Sumner, 2010). Some recent studies (Afgan et al., 2011; Chen et al., 2022; and Zeng et al., 2023) have used numerical simulation to investigate aerodynamic forces on two smooth cylinders in this arrangement for different gap ratios; however, the Reynolds numbers were limited to low Re subcritical flow ($\mathcal{O}(10^3)$). Despite differences in detail, many similar flow features observed at higher Re were observed, such as the biased flow regime, mode swapping and different flow transitions, suggesting that the geometrical setup has a much stronger effect than the flow regime.

Bearman and Wadcock (1973) reported the mean pressure distribution for $L^* = 1.5$ and the force coefficients for $L^* = \{1, 1.5, 2\}$ for smooth cylinders for a subcritical Reynolds number of $Re = 2.5 \times 10^4$. Alam et al. (2003) reported the mean and fluctuating pressure distributions and force coefficients for $L^* \leq 6$ at $Re = 5.5 \times 10^4$. To the knowledge of the authors, to date, Sun et al.

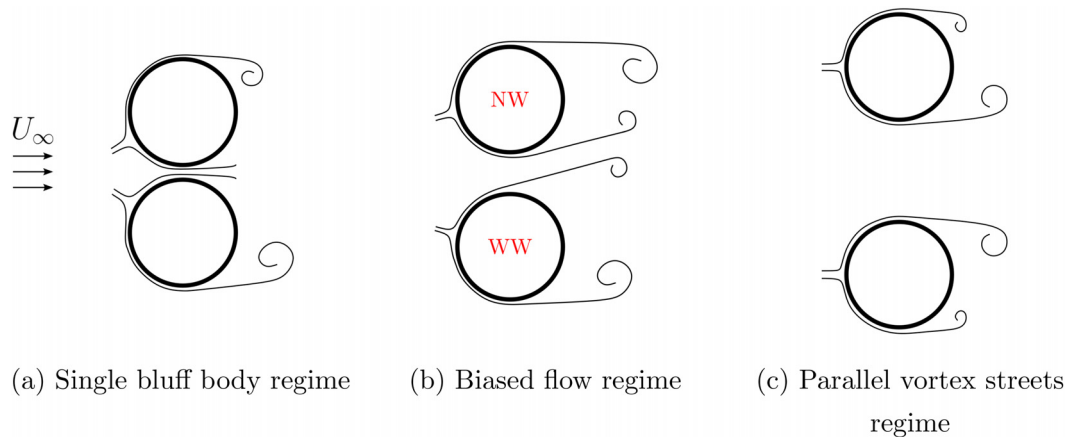


FIG. 1. Schematic representation of the flow configuration in each of the regimes.

(1992) has been the only investigation concerning the supercritical regime ($Re = 6.5 \times 10^5$) where pressure distributions were reported, but it was limited to $L^* = 2.2$.

Bearman and Wadcock (1973) found that the azimuthal location of the maximum in mean pressure, i.e., the stagnation point on the surface of a cylinder, exists at a non-zero azimuthal angle, when in proximity to another cylinder. In addition, Bearman and Wadcock (1973) also reported that the stagnation angle (referred to as θ_{st} henceforth) is larger at $L^* = 2$ than at $L^* = 1.5$. As the two cylinders are moved further away, pressure distributions on either cylinder are expected to be similar to that on an isolated cylinder, thus $\theta_{st} \rightarrow 0$ as $L^* \rightarrow \infty$. While this indicates that there could be a maxima in θ_{st} between $L^* = 2$ and $L^* = \infty$, we found that the entries of θ_{st} in table 2 of Bearman and Wadcock (1973) were interchanged, and θ_{st} at $L^* = 1.5$ was indeed greater than at $L^* = 2$.

For subcritical flow at $Re = 5.5 \times 10^4$, Alam *et al.* (2003) found that the cylinder in the NW mode experiences larger drag and lower lift while the one in the WW mode experiences lower drag and larger lift. Price and Paidoussis (1984) measured the force coefficients at $Re = 6.4 \times 10^4$ on the cylinders at various cross-stream pitch ratios while one of them was also placed $0.1D$ downstream of the other and found that the cylinder experiencing larger drag also experienced larger lift. If the side-by-side configuration can be seen as the transitional geometry when one cylinder goes from slightly upstream to slightly downstream of the other (Summer, 2010), the results of Price and Paidoussis (1984) are in contradiction to those of Alam *et al.* (2003).

More recently, Chen *et al.* (2022) and Zeng *et al.* (2023) found that the lift coefficient of the cylinder in the NW mode is larger than that in the WW mode, again, in contradiction with the findings of Alam *et al.* (2003). However, the lift coefficients found in Afgan *et al.* (2011) at $Re = 3900$, the same Reynolds number as Zeng *et al.* (2023), agree with that of Alam and Zhou (2007). Zeng *et al.* (2023) attributed the differences in the magnitude of the force coefficients with Alam *et al.* (2003) to the large difference in Reynolds numbers. The lift coefficients resulting from the two modes in a postcritical flow scenario remain uncertain. Moreover, whether the cylinder with the larger C_D also experiences the larger C_L remains unclear since it was not addressed in Chen *et al.* (2022) and Zeng *et al.* (2023), perhaps due to the sign convention followed, which resulted in opposite signs for the C_L of the two modes thus hindering a direct comparison of their magnitudes. Also noteworthy is the difference in techniques between these investigations. While Afgan *et al.* (2011), Chen *et al.* (2022), and Zeng *et al.* (2023) employed numerical simulations, Alam *et al.* (2003) used wind tunnel experiments to investigate the side-by-side arrangement.

This highlights the limitations in knowledge about crucial flow parameters and their variation with pitch ratios in the side-by-side arrangement. Providing a detailed dataset with a parameter sweep of the pitch ratio forms the primary motivation behind this investigation. In particular, we focus on quantifying flow parameters including the mean and fluctuating forces, and pressure distributions to resolve the aforementioned uncertainties.

In addition, this investigation aims to provide estimates of stagnation and separation angles for the two modes for a range of pitch ratios, both of which are crucial in understanding the flow behavior. While these parameters have been provided in the recent numerical investigations (Afgan *et al.*, 2011; Chen *et al.*, 2022; and Zeng *et al.*,

2023), experimental estimates of the same are absent. Moreover, numerical estimates are limited to low Reynolds numbers, $\mathcal{O}(10^3)$.

Importantly, this study considers postcritical flows unlike the majority of the previous investigations. While in this case postcritical flows are generated using surface roughness, previous studies on single cylinders indicate that key postcritical flow properties such as drag and lift fluctuations collapse reasonably well if the measurements are scaled according to the roughness Reynolds number (Szechenyi, 1975), especially when the effects of blockage and finite span are minimized (Pasam *et al.*, 2023).

The combination of surface roughness and Reynolds number used in the current investigation is the same as that used in a previous study of flow over two rough cylinders placed inline with the free-stream (Pasam *et al.*, 2024). This investigation forms a sub-part of the broad objective to analyze the aerodynamic interaction between two (and eventually, multiple) rough cylinders in postcritical flow. In addition, it is anticipated that these results can be extended to other surface roughnesses and Reynolds numbers using roughness Reynolds number as a similarity parameter, as described in Pasam *et al.* (2023).

The remainder of this work is divided into three sections. Section II presents the experimental setup, validation, and data processing underlying the identification of the two modes and quantification of the corresponding flow parameters. The results and discussion are presented in Sec. III, followed by the concluding Sec. IV, which highlights the key findings of this study.

II. METHODOLOGY

A. Experimental setup and data acquisition

Experiments were performed in a closed-loop wind tunnel with a test section of a rectangular cross section $4000 \times 2000 \text{ mm}^2$. Cylinders were installed vertically (2000 mm) in the test section 4600 mm downstream of the end of contraction and were rigidly mounted both to the floor and the roof. For all the tests in this investigation, the free-stream velocity was maintained at $\sim 23.2 \text{ m s}^{-1}$, thus resulting in a Reynolds number of $\sim 3 \times 10^5$, which is post critical given the roughened cylinders used (Pasam *et al.*, 2023).

Figure 2 gives the distribution of the mean velocity and the turbulence intensity in the background flow in the spanwise direction. Here, $H^* = H/D$, where H is the height of the floor. The mean velocity outside the boundary layer is within 0.5% of the global mean at the center of the test section. Turbulence intensity of the incoming flow is 1.35%. At four diameters away from the centerline in the cross-stream direction, velocity non-uniformity and turbulence intensity outside the boundary layers increase to $< 0.7\%$ and $\sim 1.8\%$, respectively. At the furthest pitch ratio tested in this investigation, cylinders were placed three diameters cross-stream from the center and seven diameters away from the sidewall.

The two cylinders were of diameter $D = 204 \text{ mm}$. They spanned the entirety of the vertical dimension, thus resulting in an aspect ratio of 9.8. The blockage ratio of a single cylinder in isolation was 5%. Both the cylinders were wrapped with a P60 grit sandpaper to provide a uniform surface roughness. This resulted in a relative roughness ratio of $k/D = 1.28 \times 10^{-3}$ and an equivalent sand-grain roughness ratio of $k_s/D = 1.9 \times 10^{-3}$. Here, k is the average sand grain diameter (provided by the manufacturer), and k_s is the equivalent sand-grain roughness that causes a similar frictional velocity deficit in a fully rough channel flow (Nikurdase, 1933). In particular, k_s is obtained

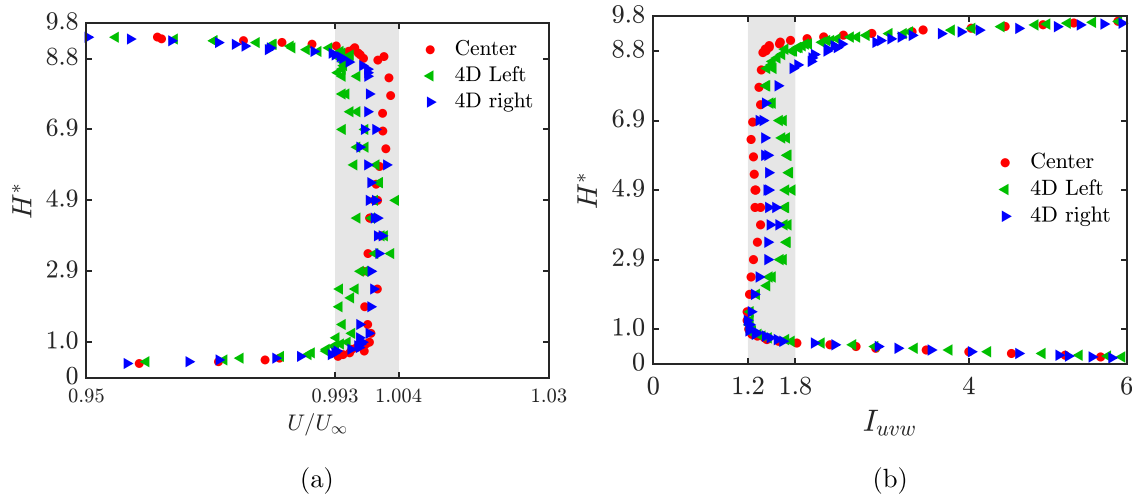


FIG. 2. (a) Mean velocity and (b) turbulence intensity distributions in the test section.

using $k_s = 1.5k$, which has been previously determined by Speidel (1954) and has typically been used in subsequent rough cylinder investigations (Achenbach, 1971; Güven *et al.*, 1980; and Pasam *et al.*, 2023).

Both the cylinders were instrumented at two cross sections, one at the midspan ($H^* = 4.9$), and another two diameters above the midspan ($H^* = 6.9$). Each cross section contained 30 equally spaced pressure measurement locations around the circumference. Pressure taps at these locations were connected to a turbulent flow instrumentation (TFI), dynamic pressure measurement system using PVC tubing, to obtain the static pressures sampled at 2000 Hz. The pressure measurements in the time domain were transformed into the frequency domain and a transfer function was applied based on the length and diameter of the tubing according to Bergh and Tijdeman (1965). The cutoff frequency for the pressure measurements was 630 Hz. For comparison, the shedding frequency of an isolated cylinder is ~ 23 Hz at $Re = 3 \times 10^5$.

Measurements were obtained for a minimum of 120 s, and each arrangement was repeated at least twice. This duration covers more than 2500 shedding cycles. Coefficients of (pressure) drag, and lift were obtained by integrating these pressures across the circumference. Further details of the setup are given in Pasam *et al.* (2023), which examined postcritical flow over a roughened single cylinder. The two cylinders used in the current investigation are the same as those in Pasam *et al.* (2024). The difference in C_D of the two cylinders at $Re = 3 \times 10^5$ is $< 1\%$.

Figure 3 gives the details of the locations of pressure measurement and the symbols used in this investigation. For the convenience of comparison, the positive direction of increase in the azimuthal angle is taken such that 270° faces the gap on both cylinders. This results in a lift coefficient that is positive outwards from the streamwise centerline. The half on each cylinder facing the gap is referred to as the *inner half*, while the half facing away is referred to as the *outer half*.

The aerodynamic force coefficients of each cylinder are represented using

$$C_{\chi\eta\alpha} = \frac{F_{\chi\eta\alpha}}{0.5\rho U_\infty^2 D}, \quad (1)$$

where $\chi \in \{D, L\}$, $\eta \in \{1, 2\}$, and $\alpha \in \{a, b\}$. Here, 1 and 2 indicate the two cylinders, while a and b indicate the locations of measurement at the midspan and two diameters above the span, respectively. Coefficients without the subscripts (η and α) are the averages of all four measurement locations. The dimensional forces, F_D and F_L , are the (pressure) drag and lift, respectively, with C_D and C_L , the corresponding drag and lift coefficients. Finally, ρ and U_∞ are the freestream density and velocity, respectively. These parameters are reported along with the corresponding 90% confidence intervals.

B. Mode separation

In the current investigation, cylinders experience both the narrow-wake and wide-wake modes for pitch ratios $1.18 \leq L^* \leq 1.75$. To analyze the modes separately, time periods for which the cylinder is in each mode are identified using the following steps.

- (i) The average of the time-mean drag coefficients measured on the two cylinders ($0.5(C_{D_1} + C_{D_2})$) is considered as a cutoff.
- (ii) Noting that the narrow-wake mode results in a larger drag than the wide-wake mode, the largest continuous instance of time for which the moving median drag coefficient (of 100 convective cycles) is larger than the cutoff is identified. The mean and standard deviation of the moving median drag are measured for this duration.
- (iii) Finally, the NW mode is identified as the period for which the moving median drag is within four standard deviations from the mean.
- (iv) If the median drag is lower than four standard deviations from the NW mode, it is considered as the WW mode. Figure 9 gives the representative results from this mode separation.

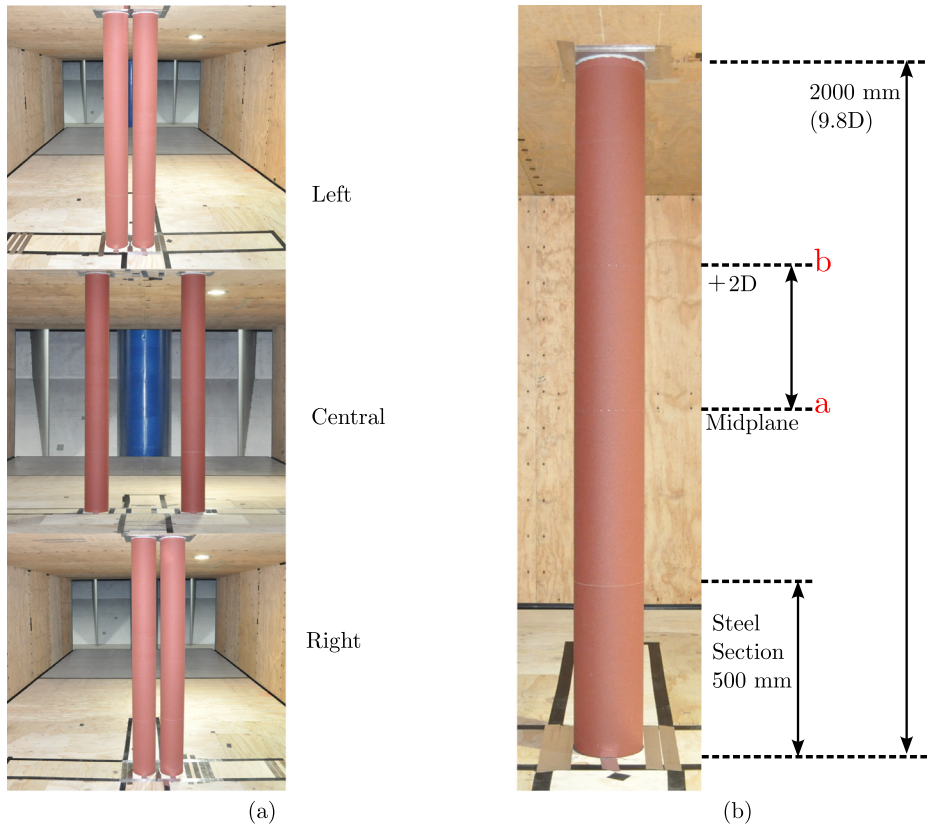
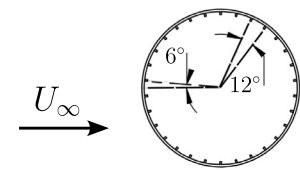
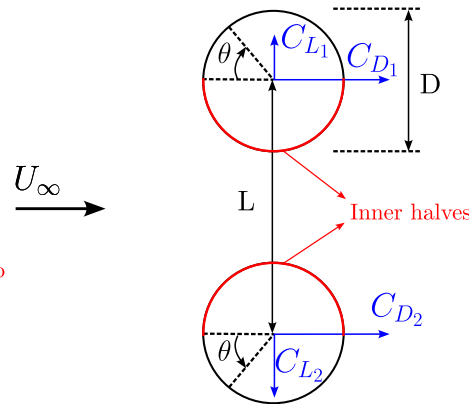


FIG. 3. Schematic of the setup. (a) Two cylinders (facing downstream), (b) and (c) measurement locations on the cylinders, and (d) notation used in this investigation.



Pressure measurement locations at a and b

(c)



(d)

- (v) For pitch ratios $L^* = \{1.18, 1.2\}$, we found intermediate modes that correspond to neither the conventional narrow wake nor the wide wake at that pitch ratio. For these pitch ratios, the time period for which a mode exists is identified for each test individually while allocating sufficient buffer near the transitions between the modes to reduce the chances of overlap. Figure 16 gives the representative result and indicates the bounds considered for each mode.

C. Parameters from the pressure distributions

Four additional parameters are used in this investigation to further analyze the pressure distribution across various pitch ratios. These are defined as follows.

- (i) The base pressure coefficient C_{p_b} is the mean pressure coefficient in the post-separation region of the cylinder.
- (ii) Wake angle $1, \theta_{w_1}$, is the point of intersection of the straight line fit in the region of pressure rise and the base pressure.

TABLE I. (a) List of pitch ratios tested in each configuration (see Fig. 3 for nomenclature), and (b) force coefficients at common pitch ratios.

Left	Right	Central	Pitch ratio	Mode	Coefficient	Left	Right	Central
1.18	1.2	-	1.5	NW	C_D	1.06	1.06	-
-	1.33	-	1.5	WW	C_D	0.87	0.86	-
1.5	1.5	-	1.5	NW	C_L	0.27	0.30	-
1.75	1.75	-	1.5	WW	C_L	0.20	0.22	-
-	1.875	-	2	NW	C_D	1.20	1.19	-
2	2	-	2	WW	C_D	1.16	1.16	-
2.25	2.25	2.25	2	NW	C_L	0.10	0.11	-
-	-	4	2	WW	C_L	0.09	0.14	-
-	-	6	2.25	-	C_D	1.18	1.17	1.17
(a)					(b)			

This serves as a good estimate for the separation angle. See [Pasam et al. \(2023\)](#) and [Güven et al. \(1980\)](#) for the procedure behind this estimate and comparison with experimental measurements of the separation angle.

- (iii) Wake angle $2, \theta_{w_2}$, is the location of the maximum in the fluctuating pressure distribution. This location is also a nominal estimate for the separation angle ([Batham, 1973](#)) and is a useful metric to further support the trends in θ_{w_1} .
- (iv) The stagnation angle, θ_{st} , is the magnitude of the shift in the stagnation point. This is estimated using a least squares fit of the curve $C_p = 1 - 4 \sin^2(\theta + \theta_{st})$ to the experimentally determined pressure coefficients in $\pm 24^\circ$ near the maximum C_p measured on the surface.

D. Validation of the geometric configurations

Due to limitations in the setup, pitch ratios of $L^* < 2.25$ could be achieved only when the two cylinders were placed asymmetrically with

respect to the wind tunnel centerline. At these pitch ratios, one of the cylinders was placed on the centerline while the other was at the cross-stream separation of L^* from the centerline. To verify and ensure that this bias had as little influence as possible, some pitch ratios were tested with the cross-stream cylinder on either side of the centerline. The three configurations are named left, right, and central, and are given in [Fig. 3](#).

Pitch ratios tested at these configurations and the mean coefficients of drag and lift from three overlapping pitch ratios are given in [Table I](#). It is evident that the two asymmetric configurations produce similar results. While the differences in C_L at $L^* = 1.5$ are relatively larger, these reflect the sensitivity of the arrangement in the biased regime toward minor asymmetries. In all subsequent figures, data from the overlapping pitch ratios from the two configurations are plotted separately so that the differences, if any, between the two are apparent in comparison with the trends reported.

III. RESULTS AND DISCUSSION

The largest pitch ratio tested in the current investigation is $L^* = 6$. At this pitch ratio, the two cylinders behave *nearly* independently. As the cylinders are moved closer, aerodynamic interaction between the two results in an increase in the mean forces and the fluctuations until $L^* = 2.25$. In addition, the aerodynamic forces on the two cylinders are the same within the experimental uncertainty until $L^* = 2.25$. A biased regime is observed below $L^* = 2.25$, resulting in a significant difference between the forces on the two cylinders at a given instant. Additionally, intermittent flow modes with lower bias than the conventional NW and WW modes are observed for $L^* \in \{1.18, 1.2\}$.

These observations are discussed through the following subsections. Sections [III A–III C](#) present the broad variation in the aerodynamic forces and the frequencies with pitch ratio. Sections [III D–III F](#) detail the parallel vortex street, the biased and the intermediate flow regimes, respectively. Section [III G](#) relates the velocity profiles measured beside an isolated cylinder and the different flow regimes in the side-by-side configuration.

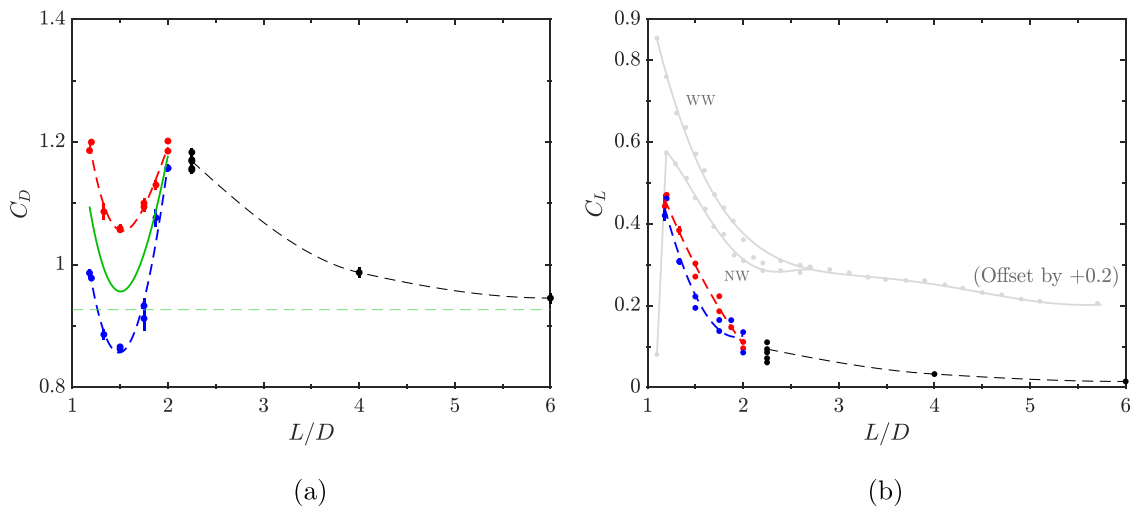


FIG. 4. Variation of (a) mean drag coefficient and (b) mean lift coefficient with pitch ratio. $Re = 3 \times 10^5$. Blue closed circle: WW; red closed circle: NW; black closed circle: parallel vortex street regime; green curve: average of drag on the two cylinders in the biased regime; green dashed line: predicted C_D of an isolated cylinder of the same roughness and for the same Reynolds number; black dashed curve: [Alam et al. \(2003\)](#), smooth cylinders, $Re = 5.5 \times 10^4$; and errors bars indicate 90% confidence intervals.

TABLE II. Mean drag and lift coefficients reported by Alam et al. (2003) at $L^* = 1.5$.

	Integration of cross-sectional pressures		Force measurements on a spanwise section	
	C_D	C_L	C_D	C_L
NW	1.14	0.44	1.03	0.26
WW	0.98	0.31	0.84	0.37

A. Mean drag and lift coefficients

Figure 4(a) gives the variation in the drag coefficient of the two cylinders with pitch ratio. Note that the current force coefficients of cylinders in the two cylinder arrangement are not corrected for wind tunnel blockage because the proposed corrections (Allen and Vincenti, 1944) do not consider the influence of wall-proximity on the interaction between the two cylinders.

Figure 4(a) also contains the corresponding predicted drag coefficient of an isolated cylinder of the same roughness and at the same Reynolds number. This is an estimate of C_D on an isolated cylinder with 10% blockage from a measurement of C_D on an isolated cylinder with 5% blockage. These corrections on the influence of wind tunnel walls are done using the method proposed by Allen and Vincenti (1944), which were later used in several investigations on flows over isolated cylinders.

As the cylinders are moved closer to large pitch ratios, the drag coefficients of each cylinder in the side-by-side arrangement agree with the experimental uncertainty for pitch ratios until $L^* = 2.25$. Thus, the parallel vortex streets regime in the current investigation exists for $L^* \geq 2.25$. This agrees well with the average estimate of $L^* > 2 - 2.2$ from the previous subcritical investigations (Sumner, 2010; Zhou and Alam, 2016) for smooth cylinders, suggesting that the influence of both the Reynolds number and the surface roughness on regime limits is minor (except in the critical Reynolds number regime).

The C_D of either cylinder in the current investigation is $\sim 7\%$ larger at $L^* = 4$ and $\sim 1.5\%$ larger at $L^* = 6$ than the predicted drag coefficient of an isolated cylinder at the same Reynolds number. For smooth cylinders at $Re = 2.5 \times 10^4$, Bearman and Wadcock (1973) found that the base pressure coefficient of a cylinder in the side-by-side arrangement matches the predicted coefficient of an isolated cylinder for $L^* = 6.2$. The results of Alam et al. (2003) at $Re = 5.5 \times 10^4$, however, indicate that the drag coefficient of either cylinder at $L^* = 6$ is similar to that of an isolated cylinder, even without accounting for changes in the blockage ratio. Blockage ratios of a single cylinder in the current investigation and in Alam et al. (2003) are 5% and 4%, respectively. Consequently, the predicted drag coefficients of isolated cylinders are $\approx 5\%$ larger than the measured drag coefficients in the two investigations. The discrepancy in the difference between the “drag coefficient of a cylinder in the side-by-side arrangement with large L^* ” and the “predicted drag coefficient of an isolated cylinder” across the two investigations is possibly due to (minor) experimental variability.

The biased flow regime in the current investigations exists for $L^* < 2.25$. In this L^* range, one of the cylinders experiences larger drag than the other for a few vortex shedding cycles. As mentioned previously, the cylinder that experiences the larger drag is in “narrow-wake mode (NW)” while the one with lower drag is in “wide-wake mode (WW).”

For flow over two smooth cylinders normal to the incoming flow in the Reynolds numbers range $2.5 \times 10^4 \leq Re \leq 1.6 \times 10^5$,

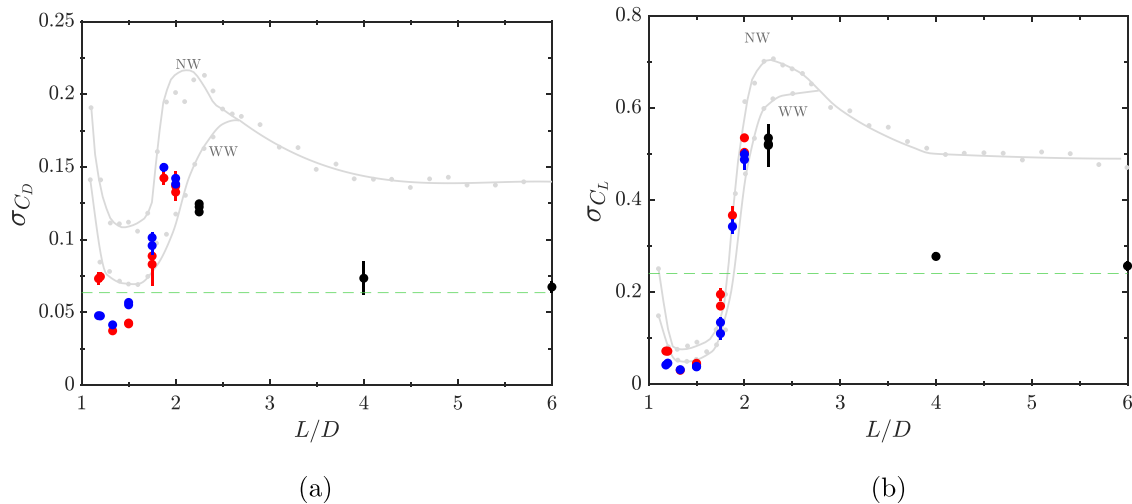


FIG. 5. Fluctuating coefficients of (a) drag and (b) lift at various pitch ratios. Blue closed circle: Fluctuations while in WW; red closed circle: fluctuations while in NW; black closed circle: fluctuations in the parallel vortex street regime; green dashed line: current, isolated cylinder under the same conditions; and Gray curve: Alam et al. (2003), smooth cylinders in the side-by-side configuration at $Re = 5.5 \times 10^4$.

13 January 2025 22:44:20

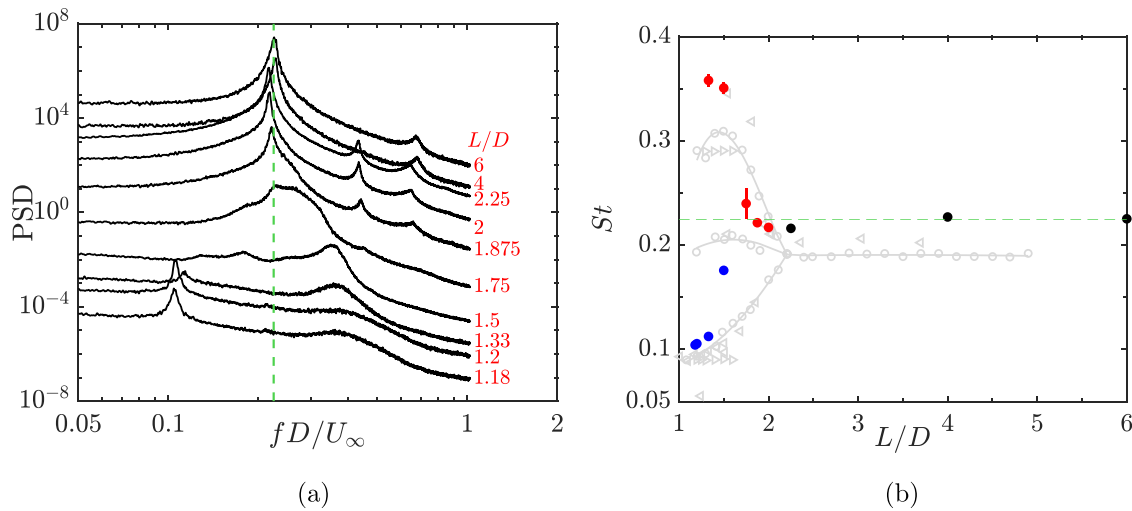


FIG. 6. (a) Power spectra of fluctuations in lift. The spectra from $L^* = 1.2$ are offset by 10 from the previous L^* to increase clarity. (b) Prominent frequencies found in the lift spectra at various separations. Blue closed circle: while in WW; red closed circle: while in NW; black closed circle: in the parallel vortex street regime; green dashed line: isolated cylinder *predicted*; Gray curve: *Alam et al. (2003)*, frequencies in the lift fluctuations, $Re = 5.5 \times 10^4$; open right triangle: *Xu et al. (2003)*, $Re = 300 - 1.4 \times 10^4$; and open left triangle: *Bearman and Wadcock (1973)*, $Re = 2.5 \times 10^4$.

Zdravkovich (1977) found that the mean of the drag coefficient of the two cylinders ($0.5(C_{D_{NW}} + C_{D_{WW}})$) in the entire biased regime is less than that of an isolated cylinder. It is uncertain whether blockage has been accounted for in their estimation of the drag coefficient of the isolated cylinder. Alam et al. (2003) found that the mean C_D is greater than that of an isolated cylinder (excluding blockage corrections) for $1.1 \leq L^* \leq 1.2$ and $2.2 \leq L^* \leq 2.5$. Current results at $Re = 3 \times 10^5$ on the smooth cylinder indicate that the mean of the drag coefficient of the two cylinders is always greater than that of the *predicted* drag coefficient of an isolated cylinder. The minimum mean of the drag coefficients of two cylinders in the current investigation is found at $L^* = 1.5$. This minimum is $\sim 3\%$ larger than the *predicted* C_D of an isolated cylinder and $\sim 8\%$ larger than the measured C_D of an isolated cylinder with 5% blockage. Zdravkovich (1977) and Alam et al. (2003) measured forces on a section of the cylinder, while the current investigation obtained force coefficients from cross-sectional pressure measurements. In addition to the differences in the Reynolds numbers and the measurement technique, the associated uncertainty with the blockage corrections could have caused this discrepancy.

Figure 4(b) gives the mean coefficient of lift at various pitch ratios. These lift forces on the cylinders are acting opposite to each other, i.e., positive lift is repulsive. At $L^* = 6$, a slightly positive lift coefficient ($C_L = 0.01$) was observed on the two cylinders. Note that a C_L of similar magnitude was also observed even on an isolated cylinder. Given this, it is possible that the non-zero lift coefficient could be due to the discrete nature of pressure measurements rather than the flow behavior at $L^* = 6$.

As the cylinders are moved closer, the repulsive lift forces increase and the largest lift force is observed at the closest pitch ratio tested. The difference between the coefficient of lift in the two modes ($C_{L_{NW}} - C_{L_{WW}}$) is smaller in the current investigation than that seen in Alam et al. (2003) for smooth cylinders at $Re = 5.5 \times 10^4$. Nevertheless, it is quite evident from the current results that the cylinder in the wide-wake mode experiences lower lift than that in the

narrow-wake mode at $L^* \in \{1.33, 1.5, 1.75\}$. For $L^* \in \{1.18, 1.2\}$ and $L^* \in \{1.875, 2\}$, the difference between the lift coefficients corresponding to the two modes is less than the experimental scatter. In contradiction, Alam et al. (2003) and Alam and Zhou (2007) observed that the WW mode results in a larger lift across all separations. Moreover, Alam et al. (2003) used the larger lift force as the filtering criterion to identify the WW mode.

To investigate this further, we integrated the mean pressure coefficients presented in Fig. 10 of Alam et al. (2003) and Fig. 2 of Alam and Zhou (2007) to obtain the cross-sectional lift coefficients. Force coefficients obtained through integration of pressure distributions and those measured on a section of cylinder [both from Alam et al. (2003)] are given in Table II. Surprisingly, the mean lift coefficient (obtained from the pressure distribution) belonging to WW is lower than that for the NW. This is in agreement with the current results but in contradiction with measurements from load cells in Alam et al. (2003).

From Table II, it is clear that there are non-negligible differences between the coefficients measured through the pressure distribution on a cross section and those using a load cell in Alam et al. (2003). The active section on which aerodynamic forces are measured by the load cell is 0.92 cylinder diameters long. Thus, the corresponding load measurements were also dependent on the spanwise correlation of the flow across this active section. However, our investigation found that the two modes are well correlated between cross sections that are two diameters apart (see Fig. 9), suggesting this is not the cause of the discrepancy.

In addition, force measurements on an entire cylinder in a slightly staggered arrangement (a streamwise separation of $0.1D$) from Price and Paidoussis (1984) indicate that the cylinder with larger drag (i.e., in the NW mode) also experiences a larger lift than that with the smaller drag (i.e., in the WW mode) for $1.25 \leq L^* \leq 3$. The Reynolds number of Price and Paidoussis (1984) ($Re = 6.4 \times 10^4$) is close to that of Alam et al. (2003) ($Re = 5.5 \times 10^4$). Both the investigations used smooth cylinders.

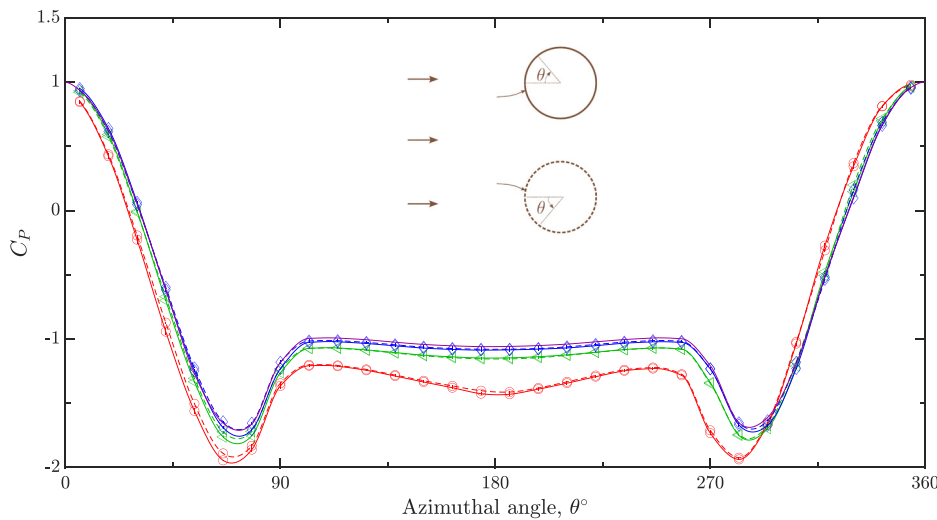


FIG. 7. Mean pressure coefficient on the surface of the two cylinders. Solid curve: cylinder 1; dashed curve: cylinder 2 (refer to inset); open red circle: $L^* = 2.25$; open green left triangle: $L^* = 4$; open blue diamond symbol: $L^* = 6$; and purple curve: predicted distribution on an isolated single cylinder.

Lift coefficients from recent numerical investigations (Chen *et al.*, 2022; Zeng *et al.*, 2023) at low subcritical Reynolds numbers ($Re = \mathcal{O}(10^3)$) are larger in magnitude than those found in the current, postcritical investigation. However, they agree with the current results in that the cylinder experiencing larger drag (i.e., NW mode) also experiences larger (magnitude) lift. In the current investigation, the difference in the lift coefficients of the two modes is small at the closest pitch ratios ($L^* \sim 1.2$), increases as the pitch ratio increases to $L^* \sim 1.75$ and diminishes for transitional pitch ratios of $L^* \sim 2$. These trends are in excellent agreement with the results of Chen *et al.* (2022) and Zeng *et al.* (2023).

To summarize, numerical investigations on low subcritical flows (Chen *et al.*, 2022; Zeng *et al.*, 2023), experimental investigations on high subcritical flows (Price and Paidoussis, 1984), and the current investigation on postcritical flows suggest that “NW mode results in larger drag, larger lift and hence a larger resultant force than the WW mode.” This contradicts the results of Alam *et al.* (2003), Alam and Zhou (2007), and Afgan *et al.* (2011) and the consequent conclusion in

the review, Summer (2010) that stated that “the NW mode has smaller C_L than the WW mode at all pitch ratios.” Of course, the current investigation studied two rough cylinders, while the rest of the investigations studied two smooth cylinders.

B. Fluctuating drag and lift coefficients

Fluctuations in the force coefficients (i.e., σ_{C_D} and σ_{C_L}) across various pitch ratios are presented in Fig. 5. Note that these coefficients do not account for increased blockage in the case of the two cylinder arrangement, since the influence of wind tunnel walls on the fluctuations of forces is uncertain. The fluctuating force coefficients at $L^* = 6$ are close to those seen for an isolated cylinder. While the asymptotic σ_{C_D} and σ_{C_L} found in the current experiments are significantly lower than those from Alam *et al.* (2003), it is worth noting that the fluctuating lift coefficient, σ_{C_L} , on an isolated rough cylinder at postcritical Reynolds numbers (Pasam *et al.*, 2023) is lower than that on smooth cylinders at subcritical Reynolds numbers (Norberg, 2003).

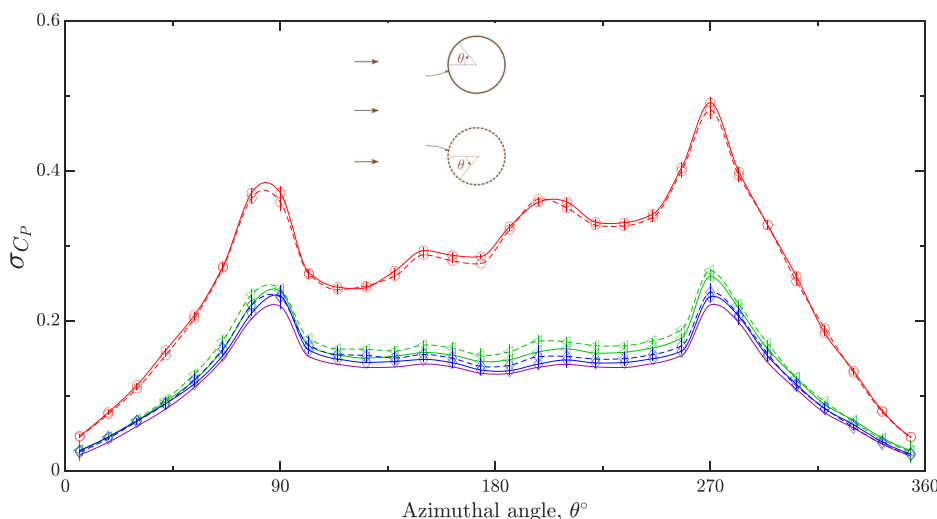


FIG. 8. Fluctuations in the pressure coefficient on the surface of the two cylinders. Solid curve: cylinder 1; dashed curve: cylinder 2 (refer to inset); open red circle: $L^* = 2.25$; open green left triangle: $L^* = 4$; open blue diamond symbol: $L^* = 6$; and purple curve: isolated single cylinder at the same Reynolds number and 5% blockage.

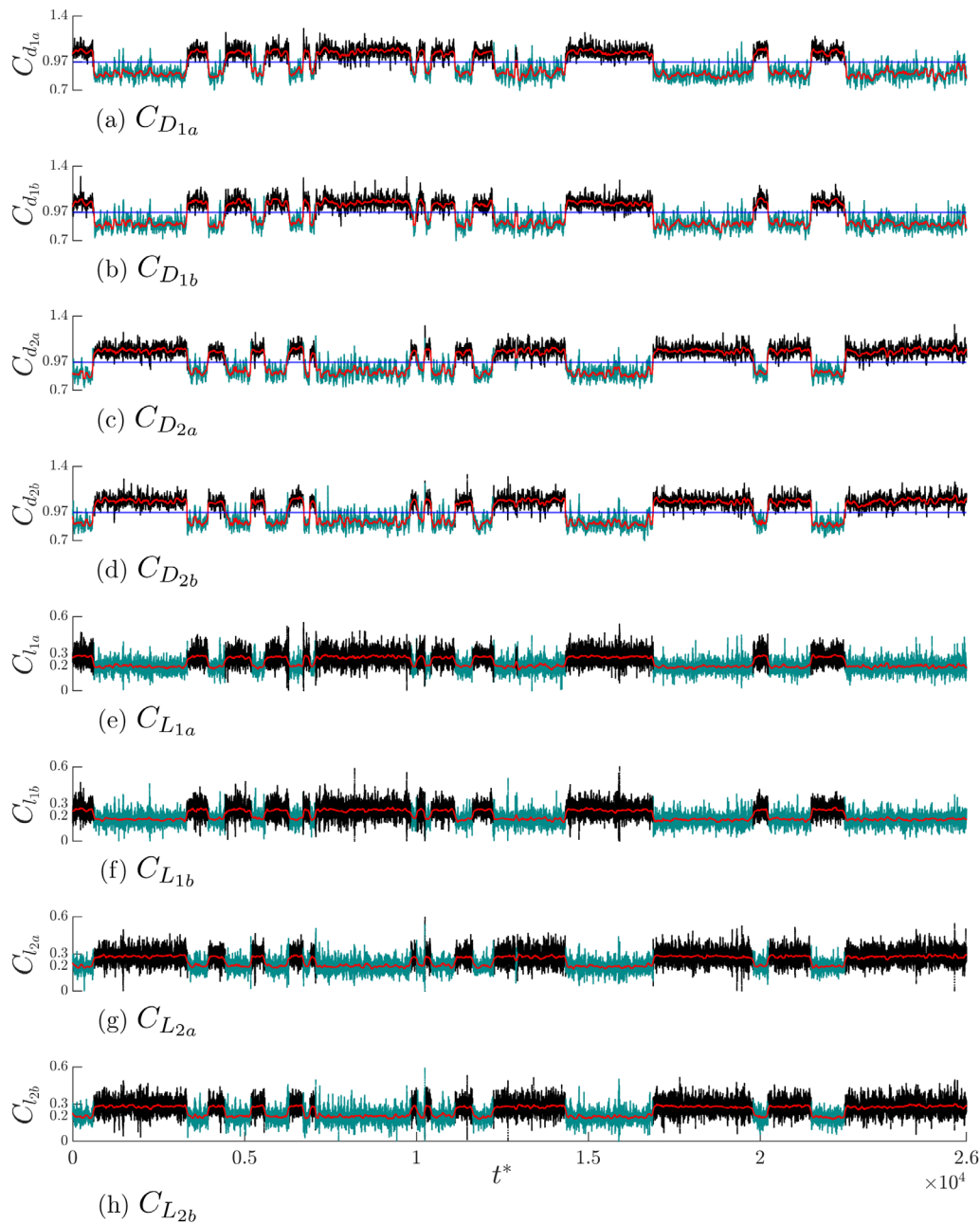


FIG. 9. Time histories of the force coefficients of the two cylinders at the two measurement planes for a pitch ratio of $L^* = 1.5$ and $Re \approx 3 \times 10^5$. Black line: narrow-wake mode; green line: wide-wake mode; red line: moving median of 100 convective time cycles; and blue line: average drag of all four locations.

As the pitch ratio is decreased from $L^* = 6$, fluctuations in both the lift and drag increase until they peak at $L^* \sim 2$; below which they reduce with decreasing pitch ratio. Note that $L^* \sim 2$ is the region of transition between the parallel shedding regime and the biased regime. The difference between drag fluctuations resulting from the narrow-wake and the wide-wake modes is much smaller in postcritical flow than those seen in subcritical flow (Alam *et al.*, 2003). Moreover, in subcritical flow, σ_{C_D} in NW is larger than that

in WW in the entire biased regime unlike the current postcritical results. At the two closest pitch ratios tested ($L^* = 1.18, 1.2$), WW results in a lower σ_{C_D} than the NW. For other L^* , WW results in larger σ_{C_D} . For lift, WW results in a slightly lower σ_{C_L} than NW at all L^* . This comparison between the fluctuating quantities of the two modes is to be considered with caution since the differences seem minor and at some pitch ratios, the difference is within the 90% confidence interval.

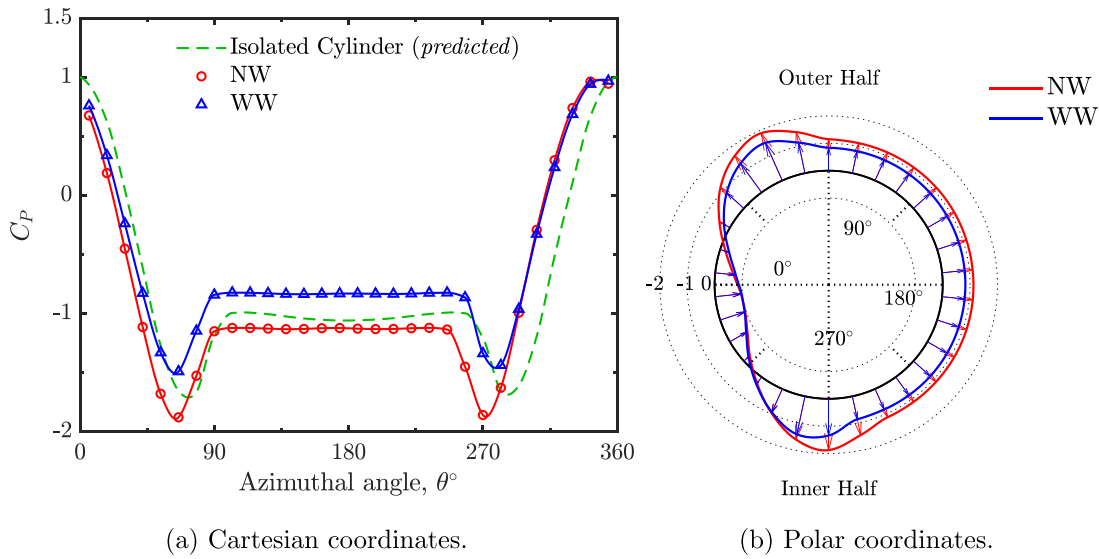


FIG. 10. Mean pressure on the surface of cylinders for the two modes at $L^* = 1.5$ and $Re = 3 \times 10^5$.

C. Spectra of lift fluctuations

Power spectra of the fluctuations in the lift coefficient of the two cylinders at different L^* are provided in Fig. 6. These spectra are the average of the four measurement locations (two on each of the two cylinders) and are also averaged across repeated tests. The averaged spectrum at the largest separation ($L^* = 6$) resembles that seen on an isolated cylinder at the same Reynolds number in that it has a prominent frequency and its third harmonic. The difference between the Strouhal number ($St = fD/U_\infty$ with f the shedding frequency) seen in a two cylinder arrangement at $L^* = 6$ and the predicted Strouhal number of an isolated cylinder is less than the experimental uncertainty. Here, the predicted Strouhal number is obtained by estimating the U_∞ at 10% blockage that would lead to the same U_∞ at no blockage,

which, in turn, is obtained from the U_∞ and C_D measured at 5% blockage and the blockage corrections proposed by Allen and Vincenti (1944).

As the pitch ratio is decreased, the second harmonic of shedding increases in prominence from $L^* = 2.25$. This second harmonic, however, is absent in $L^* \leq 1.75$. For smooth cylinders placed side-by-side with $1.6 \leq L^* \leq 1.9$ and in a much lower Reynolds number of $Re = 200$, Williamson (1985) reported second and third harmonic modes of vortex shedding in addition to the fundamental mode.

In the fundamental mode, the vortices generated from the inner halves are “squeezed and amalgamated” into the outer vortex of the cylinder in the NW mode. In the second harmonic mode of vortex shedding, the near wake contains a pair of vortices on one side and a

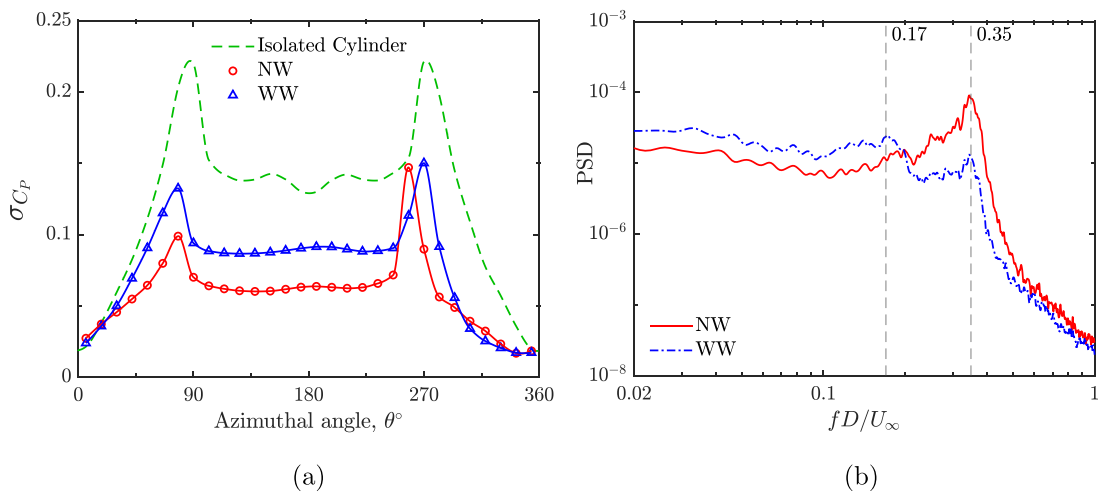


FIG. 11. (a) Fluctuating pressure distributions of the two modes at $L^* = 1.5$ and $Re = 3 \times 10^5$. (b) Spectra of fluctuations in lift for the two modes.

13 January 2025 22:44:20

single vortex on the other side of the side-by-side arrangement. The third harmonic mode is more intermittent and contains an additional weak vortex following the vortex pair. Spectra of the fluctuations in the lift in the current results confirm the prominence of second and third harmonic modes of vortex shedding from cylinders, even in the post-critical regime. Further, as pitch ratio is increased from $L^* = 1.18$, the emergence of additional harmonics (in $L^* > 1.75$) coincides with a steep increase in σ_{C_L} and σ_{C_D} , as seen in Fig. 5.

For $Re = 5.5 \times 10^4$, Alam *et al.* (2003) also found intermediate frequencies within the biased regime. However, for a given pitch ratio, the intermediate frequency was not a harmonic of the lower frequency in Alam *et al.* (2003). These intermediate frequencies were attributed to an intermittent flow configuration with an unbiased near wake behind the two cylinders—a transitional flow between the NW and the WW modes.

In this investigation, at the closest separation tested ($L^* = 1.18$), one prominent peak exists at $St \sim 0.1$, while a relatively broad plateau is seen near $St \sim 0.36$, which is close to, but not equal to the third harmonic of the lower frequency. The smaller frequency corresponds to the wide-wake mode and the larger frequency corresponds to the narrow-wake mode. A less distinct frequency is also seen at $St \sim 0.21$ (near the shedding frequency of an isolated cylinder) at $L^* = 1.18, 1.2$; this frequency corresponds to the flow configuration with a more symmetric flow in the gap. The demarcation of modes and the corresponding frequencies are given in Sec. III E.

As the pitch ratio is increased from $L^* = 1.18$, the difference between the Strouhal numbers of the two modes decreases. Energy in the frequency corresponding to the narrow-wake mode increases while that in the wide-wake mode decreases. At $L^* = 1.75$, the combination of frequencies from the two modes leads to a broad plateau in the lift spectrum. This is also seen, albeit to lesser extent, for $L^* = 1.875$. The spectrum for $L^* > 1.875$ contains one prominent frequency together with its second and third harmonics as mentioned previously.

The shear layers emanating from the inner halves of the two cylinders interact earlier at smaller pitch ratios. This suggests that the vortex structures in the shear layers near the interaction are weaker. Thus, there is a higher possibility of the formation of a stable pair of vortices in the gap at larger pitch ratios. This helps explain multiple observations in the lift fluctuations in the current investigation such as: (i) the broadband nature of the energy content near the NW frequencies in the spectra of smaller pitch ratios, (ii) the increase in the relative energy of the NW frequencies as the pitch ratio increases, (iii) the presence of prominent second and third harmonics at larger pitch ratios, and (iv) the increase in the magnitude of fluctuations in the lift coefficient at larger pitch ratios.

Unlike the force coefficients, the frequencies in the flow have been investigated extensively within the subcritical regime enabling a comparison across Reynolds numbers and different flow regimes, with the current results. Figure 6 gives the frequencies and their variation with pitch ratio across the range of Reynolds numbers in the low subcritical [$Re = 300$ in Xu *et al.* (2003)], high subcritical [$Re = 5.5 \times 10^4$ in Alam *et al.* (2003)] and postcritical regimes (3×10^5 in the current investigation). From Fig. 4(a), it is evident that the biased regime exists up to $L^* = 2$. However, only one prominent frequency exists from $L^* > 1.75$. In agreement, Bearman and Wadcock (1973) reported the biased flow up to $L^* = 2.4$ but one frequency for $L^* > 2$, and

Alam *et al.* (2003) reported the biased flow until $L^* = 2.5$ but only one frequency from 2.2.

At close pitch ratios, the ratio of the largest frequency and the smallest in the current investigation [and Bearman and Wadcock (1973)] is closer to ~ 3.5 . However, other investigations (Xu *et al.*, 2003; Alam *et al.*, 2003) reported a ratio closer to 3. It is evident from Fig. 6(a) that the energy in the higher frequency at closer pitch ratios is more broadband in nature. This lack of a sharp peak in the spectra could partially contribute to a scatter in the reported frequencies. This scatter at the larger frequency is also evident in Alam *et al.* (2003), where the frequencies from the spectra of lift, pressure, and velocity fluctuations were compared.

D. Parallel vortex streets for $L^* \geq 2.25$

The mean pressure distributions on the two cylinders at pitch ratios of $L^* \geq 2.25$ are plotted in Fig. 7. The two cylinders are distinguished to emphasize the difference in convention for azimuthal angle. The pressure distribution for the isolated cylinder is the *predicted* distribution if the blockage is increased to 10%. Similar to the drag coefficient and the Strouhal numbers, this prediction is made from the measurements on an isolated cylinder at 5% blockage using the blockage corrections proposed by Allen and Vincenti (1944).

When the cylinders are separated by $L^* = 6$, the pressure distribution resembles that of an isolated cylinder except for a minor decrease in the base pressure ($< 2\%$). Consequently, C_D of either cylinder in the two cylinder arrangement is slightly larger ($\sim 1.5\%$) than that experienced by an isolated cylinder at the same Reynolds number as seen in Fig. 4.

Thus, at $L^* = 6$, the drag coefficient of either cylinder is close to that of an isolated cylinder, and the lift coefficient and the Strouhal number are within experimental uncertainty of those predicted for an isolated cylinder. This indicates that the two cylinders are nearly independent at this pitch ratio. For two smooth cylinders, at a Reynolds number of 110, Le Gal *et al.* (1990) observed that the vortex streets from the two cylinders are phase locked even at $L^* = 6.5$. In the study of Sumner *et al.* (1999), at $Re = 3000$, they found no synchronization beyond $L^* = 4.5$.

As the cylinders are moved closer: (i) the base pressure decreases; (ii) surface pressure just upstream of the separation (and the minimum pressure) decreases; (iii) pressure on the upstream region of the inner half ($245^\circ \leq \theta \leq 360^\circ$) increases; and (iv) pressure on the upstream region of the outer half ($0^\circ \leq \theta \leq 100^\circ$) decreases.

The increase in pressure in the inner half and the decrease in the outer half as the two cylinders are moved closer suggest that the proximity to the other cylinder decelerates the flow in the gap while accelerating the flow around the outer half. Moreover, a shift in stagnation point toward the gap is also evident especially at $L^* = 2.25$. This shift in the stagnation results in the repulsive (lift) force observed in Fig. 4(b). The movement of the stagnation point also indicates a redirection of flow immediately upstream of the two cylinders. An exaggerated redirection is depicted in the inset of Fig. 7. The azimuthal shift (θ_{st}) in the stagnation point increases with the decrease in the pitch ratio and is discussed in further detail in Sec. III E.

A decrease in the minimum pressure decreases the drag force on the cylinder, while a decrease in base pressure increases the drag. The contribution to the change in drag due to decreased base pressure is more significant than that due to decreased minimum pressure, thus

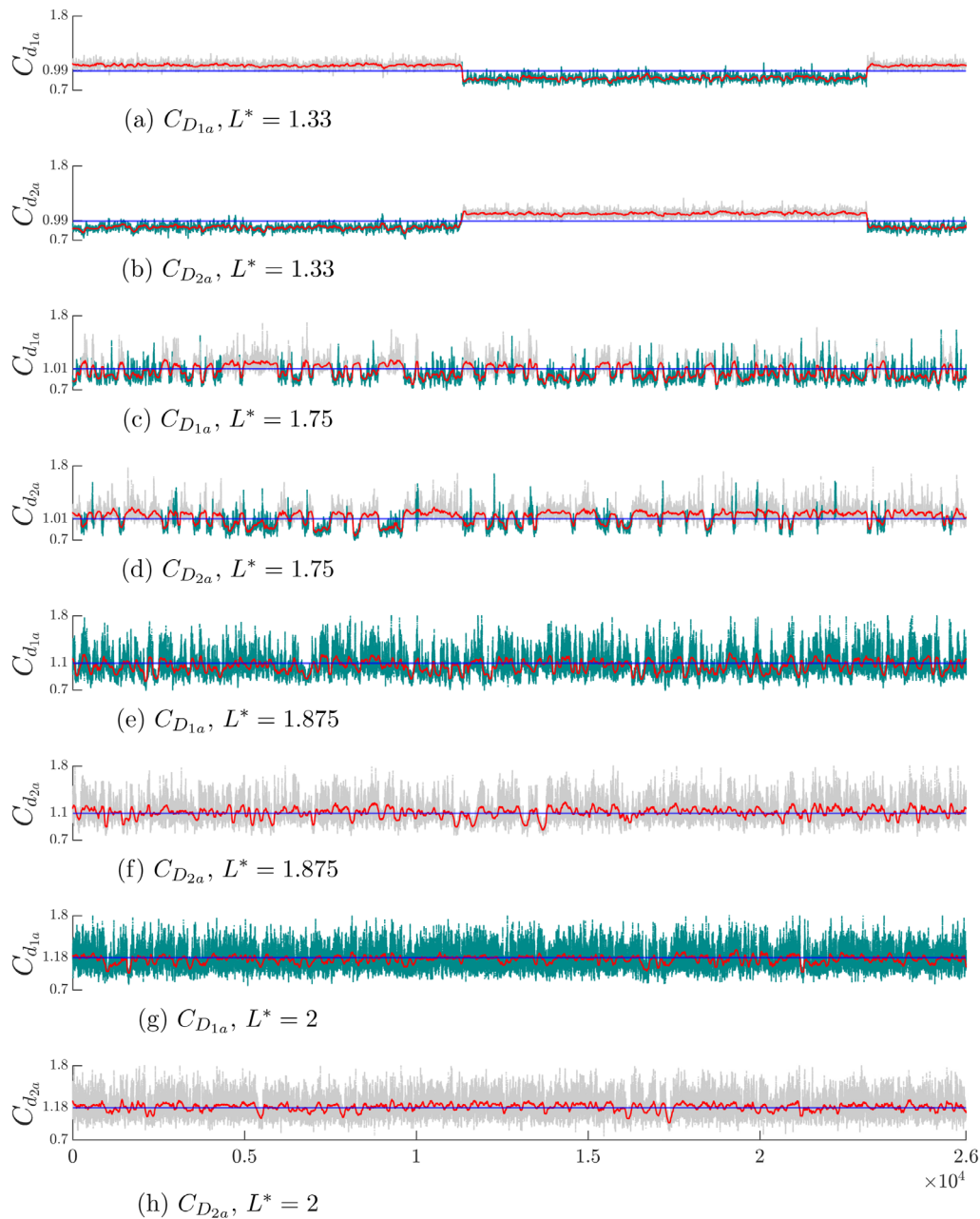


FIG. 12. Time histories of the force coefficients of the two cylinders at the two measurement planes for various pitch ratios $Re \approx 3 \times 10^5$. Gray line: narrow-wake mode; green line: wide-wake mode; red line: moving median of 100 convective time cycles; and blue line: average drag of all four locations.

resulting in an increased mean drag [see Fig. 4(a)] as the cylinders are moved closer.

Figure 8 gives the fluctuations in the surface pressure on the two cylinders for $L^* \geq 2.25$. The fluctuations for the isolated cylinder in this figure have not been corrected for blockage as the applicability of the blockage correction method in Allen and Vincenti (1944) to adjust fluctuating quantities is uncertain.

At $L^* = 6$, the fluctuations in the pressure coefficient are only slightly larger than those seen for an isolated cylinder. As the cylinder is moved closer, these fluctuations increase in the intensity and also become more asymmetric. The fluctuations in the surface pressure in the inner half are much larger than those in the outer half. Based on θ_{w_2} , the fluctuating pressure distribution implies that the boundary layer on the inner half of the cylinder separates earlier (i.e., at a larger

TABLE III. Drag coefficient on the two cylinders. *: Predicted. Note that the drag coefficients are rounded to two digits after the decimal point.

Pitch ratio L^*	Cylinder 1	Cylinder 2	% Difference
1.875	1.08	1.12	3.6%
2	1.16	1.20	3.3%
2.25	1.16	1.18	1.7%
6	0.94	0.95	0.5%
Isolated (at 5% blockage)	0.88	0.89	1%
Isolated* (at 10% blockage)	0.93	0.93	0.5%

azimuthal angle—note the convention of +ve azimuthal angle in Fig. 3) than that on the outer half when $L^* = 2.25$. Moreover, the pressure fluctuations on the base of the inner half ($180^\circ \leq \theta \leq 270^\circ$) are larger than the outer half, suggesting a closer vortex roll up in the gap.

E. Biased near wake for $L^* < 2.25$

At pitch ratios less than 2.25, the gap flow tends to be biased toward one of the cylinders for a few shedding cycles before flipping toward the other cylinder. This range of pitch ratios thus forms the “biased regime” in the current investigation. Due to the existence of two stable flow configurations at the same pitch ratio, statistics based on the total test duration, such as the time average, are insufficient to explain the underlying variations with pitch ratio. The two modes, the narrow-wake and the wide-wake modes, are separated using the procedure detailed in Sec. II, and an example is given below using the measurements at $L^* = 1.5$.

1. The two modes at $L^* = 1.5$

The force coefficients measured on the four cross-sectional planes at $L^* = 1.5$ are plotted against the convective time ($t^* = tU_\infty/D$) in

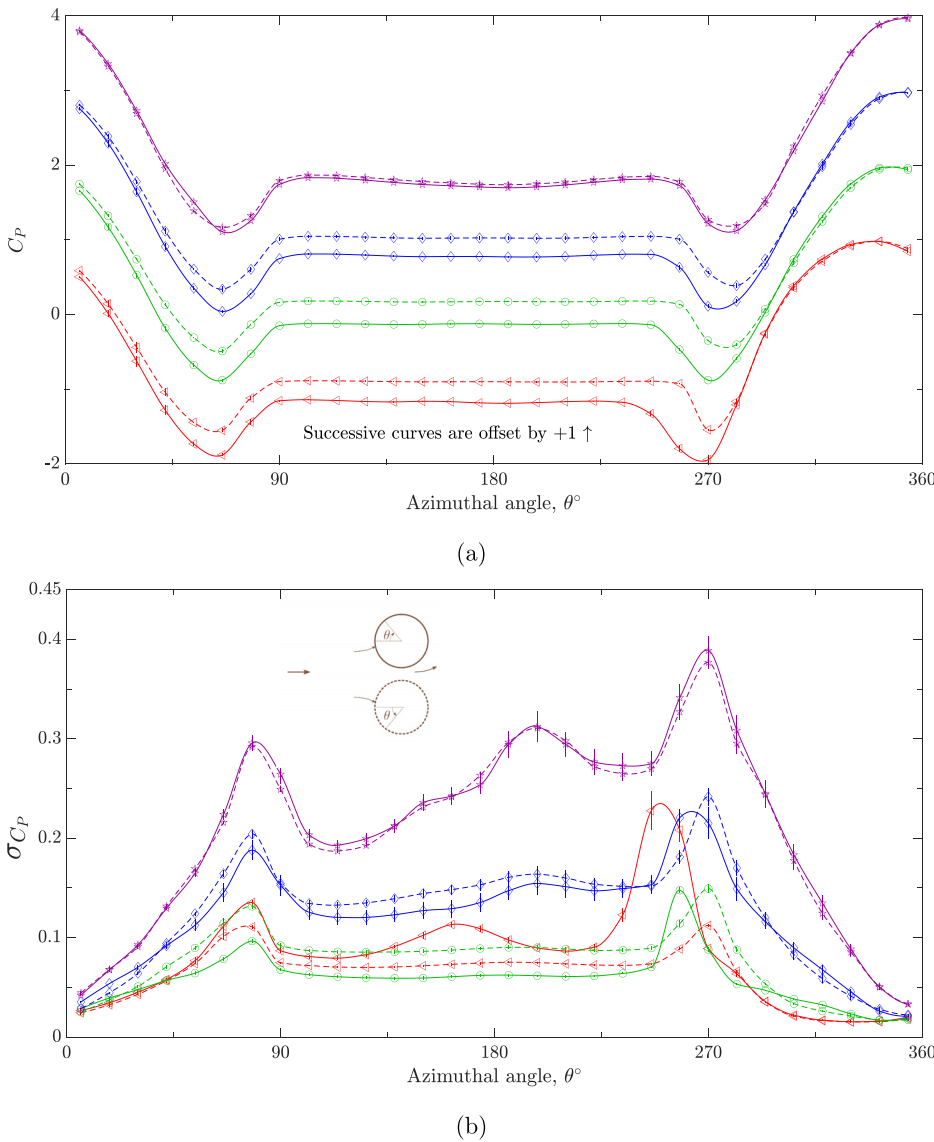


FIG. 13. (a) Mean and (b) fluctuating pressure coefficients on the surface of the two cylinders at $Re = 3 \times 10^5$. Open left red triangle: $L^* = 1.18$; open green circle: $L^* = 1.5$; open blue diamond symbol: $L^* = 1.75$; star purple symbol: $L^* = 1.875$; the solid line represents the NW mode; and the dashed line represents the WW mode.

13 January 2025 22:44:20

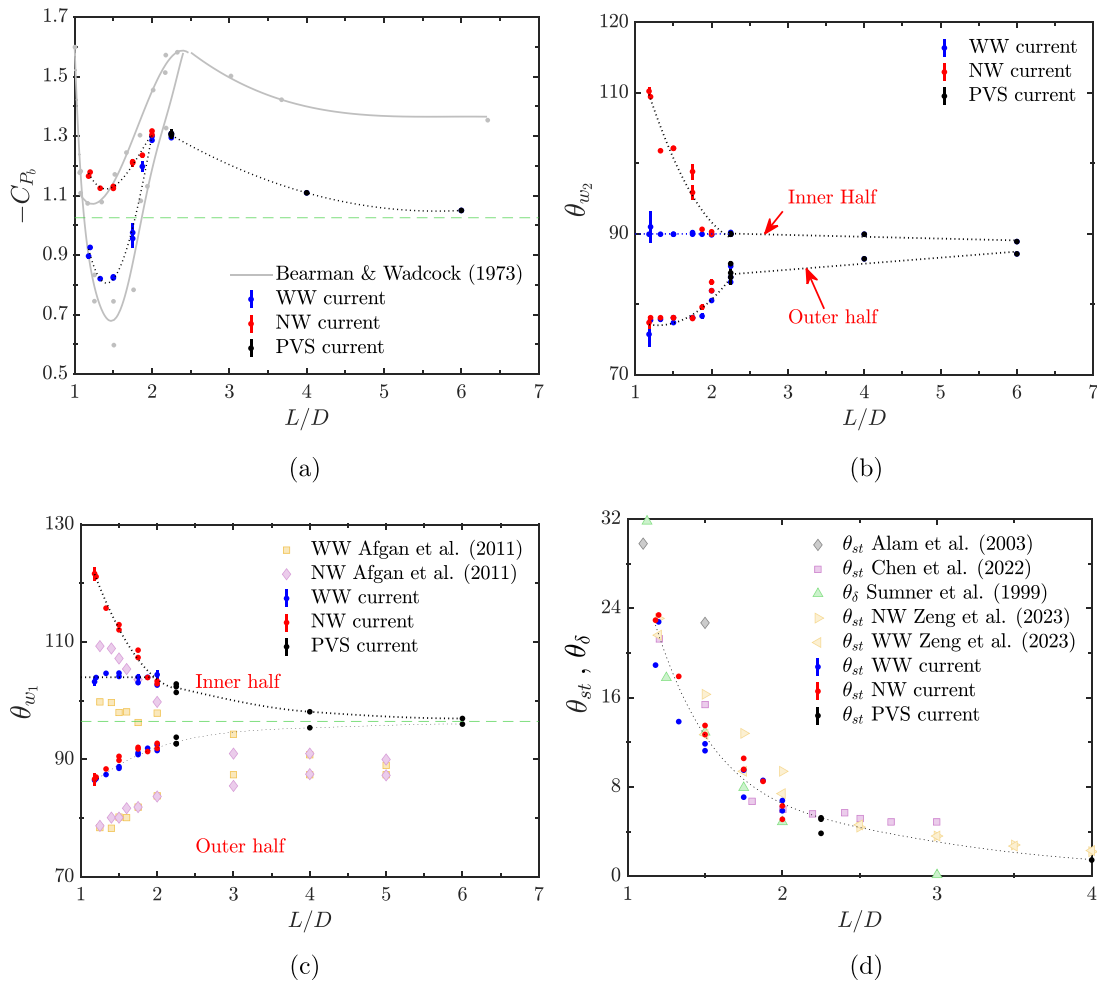


FIG. 14. (a) Base pressure; (b) and (c) wake angles and (d) stagnation and deflection angles across various pitch ratios. Green dashed line: Isolated cylinder (predicted for 10% blockage); - - - - -: Mean curves from the current data.

Fig. 9. Evident from this figure is that the transitions between modes occur in an unpredictable manner. In addition, the larger drag (narrow-wake mode) corresponds to the larger lift. As mentioned previously, this is contrary to results from Alam *et al.* (2003) and Afgan *et al.* (2011) but in agreement with those from Price and Paidoussis (1984), Sumner *et al.* (2005), Chen *et al.* (2022), and Zeng *et al.* (2023).

Figure 9 also demonstrates a spanwise coherence in mode switching, as when a particular mode exists, it exists on both cross sections of the cylinder (separated along the span by two diameters). This is observed not only at $L^* = 1.5$ but also at $L^* = 1.33$ and 1.75 . This indicates that the C_L on the section spanning the two diameters (and presumably, the entirety) of the cylinder is lower during the wide-wake mode than during the narrow-wake mode for these pitch ratios.

TABLE IV. List of investigations compared in Fig. 14.

Investigation	Methodology	Reynolds number
Afgan <i>et al.</i> (2011); Zeng <i>et al.</i> (2023)	Numerical simulations, smooth cylinders	3900
Chen <i>et al.</i> (2022)	Numerical simulations, smooth cylinders	500
Bearman and Wadcock (1973)	Wind tunnel experiments, smooth cylinders	2.5×10^4
Alam <i>et al.</i> (2003)	Wind tunnel experiments, smooth cylinders	5.5×10^4
Current	Wind tunnel experiments, rough cylinders	3×10^5

Figure 10 gives the mean pressure distribution on the surface of the two cylinders for the two modes. The average of surface pressure distributions of the four measurement cross sections is presented in both Cartesian [Fig. 10(a)] and polar [Fig. 10(b)] coordinates.

Comparing the two modes, the difference between the base pressures contributes to the difference in the drag coefficient. Except within $245^\circ \leq \theta \leq 360^\circ$, the flow near the surface of the cylinder in the NW mode accelerates more than that in the WW mode, thus resulting in higher velocity and hence lower surface pressure. This is also evident in the significantly lower minimum pressure on the cylinder in the NW mode on both the halves.

A prominent difference between the (cross-stream) pressures in the two modes can be observed within $18^\circ \leq \theta \leq 90^\circ$ in the outer half and $258^\circ \leq \theta \leq 282^\circ$ in the inner half of the cylinder. The difference in pressure between the two modes, i.e., $|C_{P_{NW}} - C_{P_{WW}}|$, in the outer half is larger than that in the inner half. Consequently, the NW mode results in a larger cross-stream force toward the outer half, i.e., larger repulsive lift than for the WW mode.

Figure 11(a) gives the fluctuating pressure distribution for the two modes. Note that the fluctuations in pressure on the isolated cylinder are measured at 5% blockage. Pressure fluctuations over the entire circumference of the cylinder are smaller than those seen on an isolated cylinder for both the modes. Consequently, σ_{C_t} and σ_{C_d} in the side-by-side arrangement at $L^* = 1.5$ are smaller than those observed on an isolated cylinder. In the base region of the cylinder, the fluctuations in the WW mode are larger than those seen in the NW mode. This contributes toward larger σ_{C_d} for WW than NW at this pitch ratio and is seen in Fig. 5(a).

The immediate wake of the cylinder in either mode is more quiescent than that of an isolated cylinder. The mean pressure distribution on the base of cylinders in both modes is flatter when compared to that seen on an isolated cylinder. Moreover, the fluctuations in pressure on the base of the cylinders in both modes are smaller than those observed for an isolated cylinder.

Figure 11(b) presents the spectra of the fluctuations in the lift coefficient at $L^* = 1.5$. These spectra are obtained from time intervals when a particular mode exists in the time history corresponding to Fig. 9. The narrow-wake mode contains a prominent frequency at $fD/U_\infty \sim 0.35$, while the wide-wake mode has two prominent frequencies, at $fD/U_\infty \sim 0.17$ and at $fD/U_\infty \sim 0.35$ (of lower prominence). This indicates that the larger frequency found in the spectra presented earlier in Fig. 6(a) corresponds to NW and the smaller frequency corresponds to WW.

2. Variation of the two modes with pitch ratio

Figure 12 provides the time history of the drag coefficients at the mid span of the two cylinders at various pitch ratios. These time histories are provided to demonstrate the nature of flip flopping between the two modes within the biased regime.

Along with the instantaneous drag coefficients, a moving median drag coefficient (of 100 convective cycles) and the average drag of the four measurement locations are also highlighted. For pitch ratios of $L^* \in \{1.33, 1.5, 1.75\}$, the two modes are easily distinguishable and are separated using the procedure detailed in Sec. II B.

As the pitch ratio is increased, the difference in drag between the two modes decreases. In addition, the time period for which a particular mode exists also decreases. The mean drag coefficients of the two

cylinders at various pitch ratios are provided in Table III. The difference in the mean drag between the two cylinders for $L^* = 1.875, 2$ is larger than that seen when they are isolated. This indicates that the flow in the gap is biased for these pitch ratios.

At closer pitch ratios ($L^* = 1.2\text{--}1.8$) and for lower Reynolds numbers ($Re \sim \mathcal{O}(10^3)$), Chen *et al.* (2022) and Zeng *et al.* (2023) found that the bias in the near wake is stable and does not flip flop. This can be attributed to the smaller simulation time in the numerical investigations. Transient force coefficients reported by Chen *et al.* (2022) and Zeng *et al.* (2023) spanned ~ 1000 convective cycles (t^*). It is evident from the current investigation (Figs. 9 and 12) that the near wake bias is stable for longer than $t^* \sim 10^3$ at closer pitch ratios.

For $L^* = 1.875, 2$, the two modes are not easily distinguishable from their time histories alone in the current investigation. Moreover, the gap flow appears to be stably biased toward one cylinder for the majority of the test duration instead of flip-flopping. Thus, for these pitch ratios, the cylinder with the larger time mean drag coefficient is considered to be in the NW mode for the entirety of the test and that with the smaller drag coefficient is considered to be in the WW mode.

Noting that the setup in the current investigation is asymmetric with respect to the wind tunnel centerline for $L^* < 2.25$, it is uncertain from the current results whether the stably biased flow at $L^* = \{1.875, 2\}$ is inherent to flow over two cylinders placed beside each other. The small difference in mean drag coefficients of the two modes in the left and right configurations indicates that the inherent asymmetry with the setup has only a minor influence, if any.

Figure 13 presents the surface pressure coefficients resulting from the two modes within the biased regime. Note that these pressure coefficients are averages from the four measurement locations and repeated tests. However, for the sake of clarity, the lower cylinder is assumed to be in the wide-wake mode. The convention for the azimuthal angle stays the same as for Figs. 7 and 8.

The mean pressure distribution for the two modes in the biased regime is given in Fig. 13(a). Supporting the time histories in Fig. 12, the difference between the two modes decreases as the pitch ratio increases. At $L^* = 1.875$, the mean pressure distributions arising from the two modes are relatively similar except for the wide-wake mode experiencing a slightly larger base pressure that results in slightly lower drag.

Continuing from the parallel vortex regime (Fig. 7), a decrease in the pitch ratio causes a further shift in the stagnation point of the cylinder toward the gap. As the two cylinders are moved closer from $L^* = 1.75$, the similarity in the pressure distributions in the inner half of the two modes also extends further downstream. The mean pressure distributions of the two modes deviate at $\sim 270^\circ$ for $L^* = 1.18$, while they deviate at $\sim 294^\circ$ for $L^* = 1.75$.

Figure 13(b) gives the fluctuating pressure distribution for various pitch ratios in the biased regime. No prominent distinction is seen in the fluctuating pressures for two modes for $L^* = 1.875$. Fluctuations in the base region for the WW mode are larger than those seen for the NW mode for $L^* = 1.5$. However, this trend reverses for $L^* = 1.18$. The NW mode for $L^* = 1.18$ exhibits much larger fluctuations in the pressure than the WW mode. Moreover, a local region of large fluctuations exists in the base region of inner half, i.e., over $125^\circ \leq \theta \leq 180^\circ$, indicating a vortex roll up closer to the surface of the cylinder.

This irregular variation across pitch ratios results in uncertain trends in the variation of σ_{C_d} between the two modes, as seen in

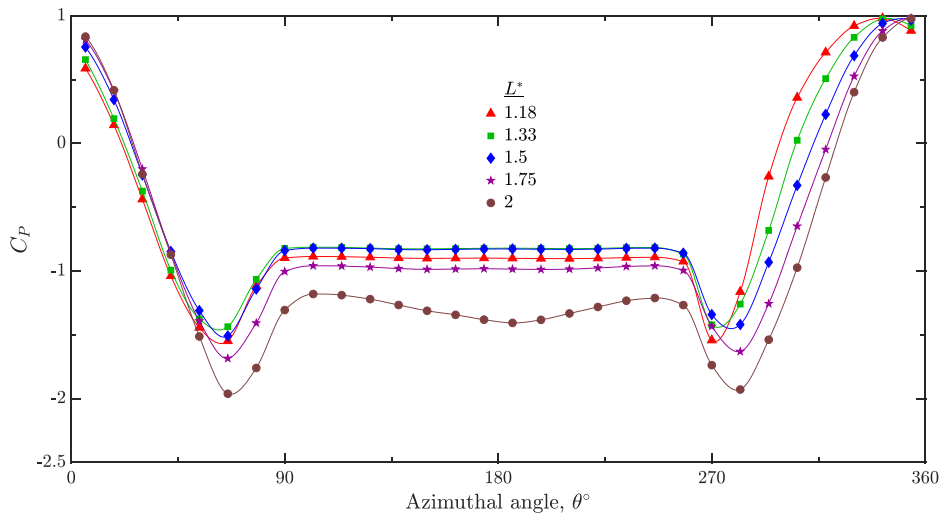


FIG. 15. Mean pressure coefficient on the surface of the two cylinders when in the WW mode.

Fig. 5(a). However, it is evident that the fluctuations over the circumference increase with pitch ratio from $L^* = 1.5$ for both modes. This results in an increase in σ_{C_D} and σ_{C_L} with increasing pitch ratio from $L^* = 1.5$.

The coefficient of base pressure, the estimates of the separation angle and stagnation angle for various pitch ratios are plotted in Fig. 14 and the details of previous investigations compared in the figure are given in Table IV.

It is evident from Figs. 4(a) and 13(a) that the variation in the drag coefficient with pitch ratio closely follows the variation in the (negative) base pressure coefficient. Current trends in C_{P_b} agree well with those reported by Bearman and Wadcock (1973) for smooth cylinders at $Re = 2.5 \times 10^4$.

The two wake angles θ_{w_2} and θ_{w_1} are presented in Figs. 13(b) and 13(c), respectively. These angles provide useful estimates for the angle at which the boundary layer separates from the surface of the cylinder. Both the estimates suggest that the boundary layer separation occurs further downstream on the inner half than on the outer half, regardless of the mode. Consequently, a cross-stream force toward the outer half (i.e., repulsive lift) is observed at all pitch ratios. The difference between the separation angles on the two halves increases as the pitch ratio decreases, thus increasing the lift coefficient in both modes.

At all pitch ratios, the separation angle on the outer half is upstream of that seen for an isolated cylinder, while it is always downstream on the inner half. At the same azimuthal location, the boundary layer on the cylinder is expected to be thinner on the inner half than that on the outer half, since it travels a shorter distance on the surface of the inner half due to the movement of the stagnation point toward the inner half. This results in a later separation of the inner half.

Moreover, the boundary layer separates at a similar location for both modes on the outer half. On the inner half, however, flow separation occurs earlier while in the WW mode than in the NW mode. Interestingly, the location of separation for the WW mode on the inner half remains nearly constant across the biased regime. On the other hand, the separation angle for the NW mode on the inner half decreases with increasing pitch ratio.

Also provided in Fig. 13(c) are the estimates of the boundary layer separation angles from the numerical investigation of two

smooth cylinders placed side by side at $Re = 3900$ (Afgan *et al.*, 2011). For a given pitch ratio, wake angles identified in the current investigation are larger than the separation angles in Afgan *et al.* (2011) by $\approx 10^\circ$. Prominent differences in Reynolds number and surface roughness could be the reason behind this difference. More importantly, the trends in the separation angle from both investigations are in excellent agreement, i.e., boundary layer separation on the outer half is similar for the two modes and occurs later as pitch ratio is increased, the boundary layer corresponding to the WW mode in the inner half separates at a similar azimuthal location across the biased regime, and the boundary layer corresponding to the NW mode separates further downstream than the WW mode and earlier as pitch ratio is increased.

Figure 13(d) indicates that the flow close upstream of the cylinder deflects toward the inner half as the cylinders are moved closer to each other. At the closest separation tested, θ_{st} , which is the deviation in the stagnation angle, is as large as $\sim 24^\circ$.

The variation of the azimuthal location of stagnation between the two modes requires further clarification. Current results indicate a non-negligible difference in the stagnation point locations between the two modes in the biased regime. The WW mode results in a lower stagnation angle when compared to the NW mode. Zeng *et al.* (2023), for two smooth cylinders at $Re = 3900$, reported a similar trend. However, Chen *et al.* (2022) averaged the stagnation angles between the two modes, perhaps suggesting that there is no significant deviation between the two for a given pitch ratio.

Using particle image velocimetry (PIV), Sumner *et al.* (1999) estimated the deflection angle of the near wake behind two smooth cylinders in the side-by-side arrangement at $Re = 1200$ – 3000 . These wake deflection angles θ_δ vs pitch ratio are also plotted in Fig. 13(d). Note that θ_δ presented here are the mean values from Sumner *et al.* (1999) and the instantaneous wake deflection oscillates with a non-negligible amplitude.

It is evident that the mean deflection in the near wake is close to the deviation in the stagnation angle toward the inner half. In addition, $\theta_{w1} - \theta_{w1,isolated}$ is within 5° of θ_{st} for the NW mode in the inner half (in the current results). This suggests that in the inner half, the NW mode is similar to the flow on an isolated cylinder with an additional rotation imparted to the stagnation, separation and the wake deflection angles.

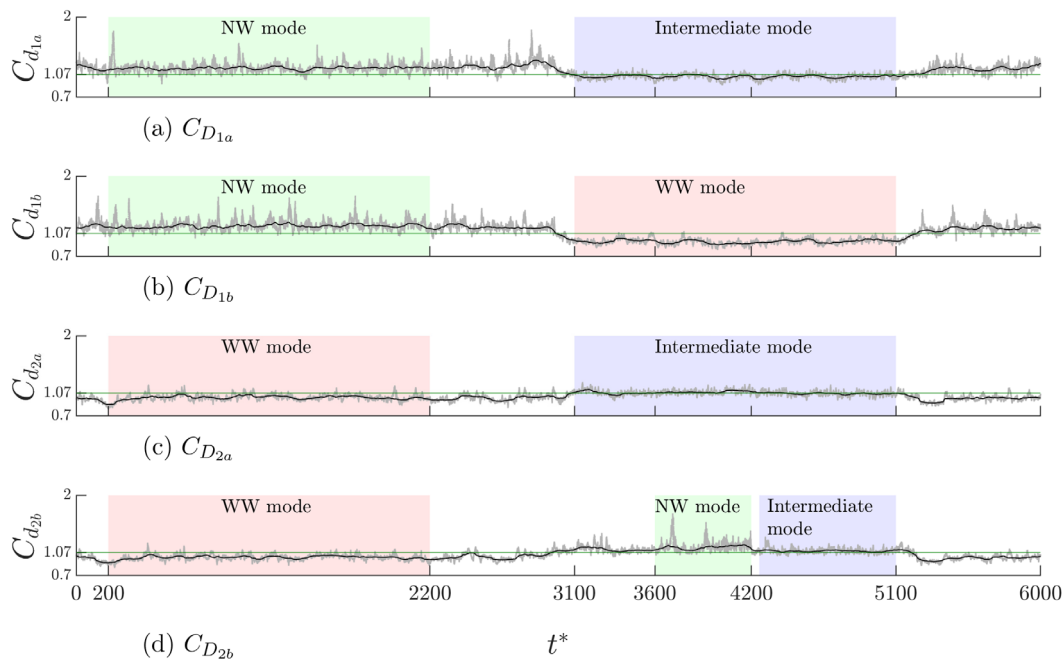


FIG. 16. Time histories of the drag coefficients of the two cylinders at the two spanwise measurement planes for $L^* = 1.18$ at $Re \approx 3 \times 10^5$. Green line: time-average drag (average of all four locations). Black line: Moving median of 100 convective cycles.

The WW mode, however, separates at a similar angle in the inner half across pitch ratios despite the deviation in the stagnation point.

As mentioned previously, entries of θ_{st} for $L^* = 1.5, 2$ in table 2 of Bearman and Wadcock (1973) were interchanged. The estimates from Bearman and Wadcock (1973) after correcting agree with the current estimates. Alam et al. (2003) found a larger deflection in the flow at $L^* = 1.5$ than observed in the other investigations, and the reason for this difference is uncertain. Note, however, that the stagnation angles from Alam et al. (2003) are our estimates from the reported mean pressure distribution plots and are not direct reported measurements from that study.

Interestingly, neither the stagnation angle nor the separation angle have saddle points in $1.18 \leq L^* \leq 2.25$. However, a minimum in $-C_p$, and hence, in C_D , exists near $L^* \sim 1.5$ for both the NW and WW modes in the current investigation. A minimum in C_D with varying pitch ratio in the biased regime also exists in the case of flow over two square cylinders placed side-by-side (Alam et al., 2011). This further suggests that the C_D minimum is not related to the variation in the location of boundary layer separation with pitch ratio.

Bearman (1967) noted that the base pressure of a bluff body is closely related to the entrainment within its wake region, i.e., the region enclosed by the separated shear layers. An increase in the entrainment in the near wake reduces the base pressure and vice versa. A reduction in the base pressure would cause an increase in the drag.

Compared to cylinders that are in contact ($L^* = 1$), an increase in pitch ratio allows the passage of low momentum fluid through the gap (Bearman and Wadcock, 1973). The low momentum fluid supports some of the entrainment required by the shear layers thus reducing the same within the wake. This results in a downstream movement of the vortex formation region, thus increasing the base pressure and

decreasing the drag. Beyond a certain pitch ratio, a further increase in the gap allows higher-momentum fluid to pass through, which entrains fluid from the shear layers thus inducing an earlier vortex roll up.

The mean pressure distributions on the surface of the cylinder at various pitch ratios further help to demonstrate this effect since the pressure on the surface of the cylinder in the inner half is indicative of the velocity of the flow through the gap.

The mean pressure distributions in the WW mode at various pitch ratios are presented in Fig. 15. Here, the WW mode is chosen over the NW mode since the variation in C_p is expected to be more pronounced as the variation in C_D of the WW mode in the biased regime is larger [Fig. 4(a)].

Substantiating (Bearman and Wadcock, 1973), the minimum pressure in the inner half varies non-monotonously with pitch ratio in the biased regime. With an increase in the pitch ratio from $L^* = 1.18$, the minimum pressure increases until $L^* = 1.5$. Bleed flow with low-momentum fluid in the gap results in an increase in pressure. On further widening the gap from $L^* = 1.5$, high-momentum fluid in the gap results in a decrease in pressure in the inner half.

The variation of the base pressure is inline with the minimum pressure, i.e., base pressure increases from $L^* = 1.18$ to $L^* = 1.5$ and decreases beyond that. Concomitant with $-C_p$, the drag coefficient forms a minimum at $L^* = 1.5$

F. Intermediate modes in $L^* = 1.18, 1.2$

Figure 16 presents the drag coefficients measured in an interval of the sampling period against convective time for $L^* = 1.18$. It demonstrates the existence of an intermediate mode in the near wake (in addition to the conventional NW and WW modes).

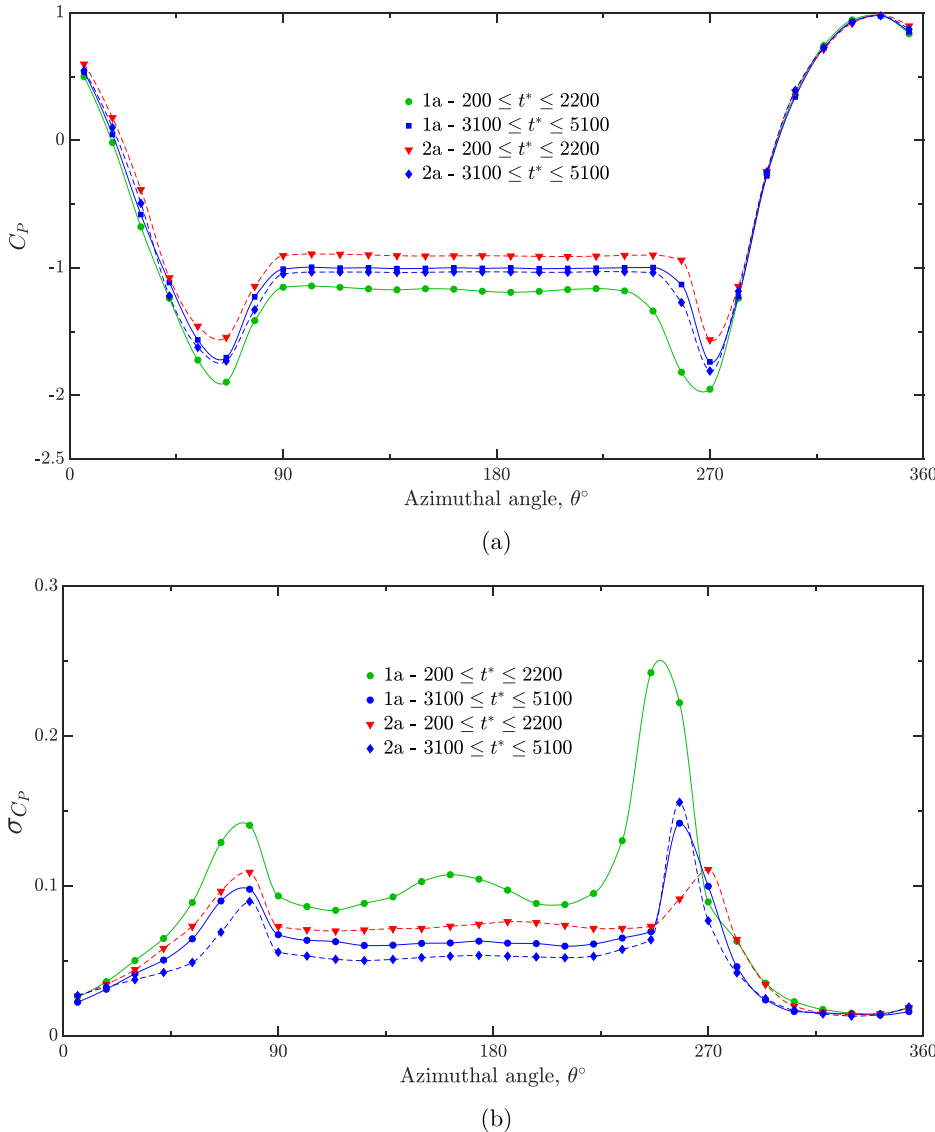


FIG. 17. (a) Mean and (b) fluctuating pressure coefficients on the surface of the two cylinders at $Re = 3 \times 10^5$ in the time periods shown in Fig. 16.

Three periods are highlighted in the figure.

- (1) The NW mode when the median drag coefficient is larger than the time-mean drag over the sampling period, e.g., $C_{D_{1a}}$ in $200 \leq t^* \leq 2200$.
- (2) The WW mode when the median drag coefficient is lower, e.g., $C_{D_{2a}}$ in $200 \leq t^* \leq 2200$.
- (3) An intermediate mode where the drag coefficient is either less than $C_{D_{NW}}$ or greater than $C_{D_{WW}}$, thus leading to a difference in median drag of the two cylinders that is smaller than $C_{D_{NW}} - C_{D_{WW}}$ but is non-negligible, e.g., $C_{D_{1a}}, C_{D_{2a}}$ in $3100 \leq t^* \leq 5100$.

These time intervals span more than 1000 convective cycles (i.e., more than 100 shedding cycles at the WW frequency), indicating that the flow pattern in each of these intervals is stable. Note that the

conventional high-drag and low-drag refer to the “NW mode” and the “WW mode,” respectively, while the stable modes that result in drag between the extremes are collectively referred to as “Intermediate modes.” The NW, the WW, and the intermediate modes are due to the maximum bias toward, maximum bias away and intermediate biases, respectively, from the cylinder.

While in the intermediate mode in $3100 \leq t^* \leq 5100$, the difference in the time-mean drag of the two corresponding cross sections at the midplane (i.e., $C_{D_{1a}} - C_{D_{2a}}$) is $\approx 4\%$ of the mean drag. In comparison, $C_{D_{NW}} - C_{D_{WW}}$ is $\approx 16\%$ of $0.5(C_{D_{NW}} + C_{D_{WW}})$. This suggests that the gap flow, while in the intermediate mode is less biased than that in the two more conventional wake modes (NW and WW). Moreover, the non-negligible difference between the drag coefficients in the intermediate mode indicates that although the bias is small, it is still non-zero.

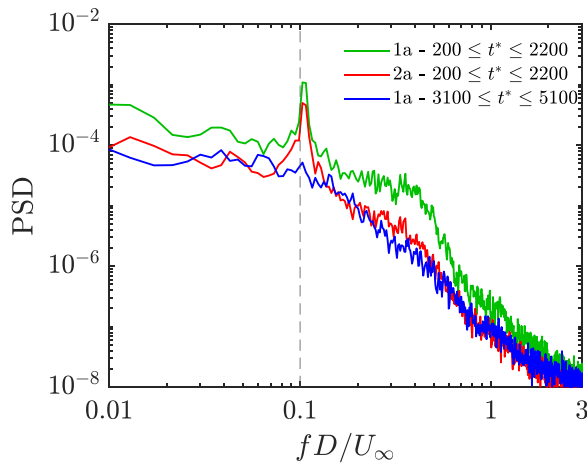


FIG. 18. Spectra of fluctuations in lift in the time periods shown in Fig. 16.

The mean and fluctuating pressure coefficients for the corresponding time periods in Fig. 16 are given in Fig. 17. It is evident that in $200 \leq t^* \leq 2200$, cylinder 1 is in the NW mode with a lower mean base pressure, larger fluctuations, and later separation in the inner half. On the other hand, cylinder 2 is in the WW mode with a larger mean base pressure, lower fluctuations, and earlier separation in the half facing the gap.

The pressure distribution and the corresponding force coefficients in $3100 \leq t^* \leq 5100$ are different from both the narrow-wake and wide-wake distributions. The difference between the base pressures on the two cylinders is small compared to that between the narrow-wake and wide-wake modes. This results in a smaller difference in the drag coefficients.

In addition, over $200 \leq t^* \leq 2200$, the gap flow is biased over both the cross sections. On the other hand, in $3100 \leq t^* \leq 5100$, gap flow is less biased in the cross section at mid span. In the cross section at $+2D$, cylinder 1 is in the WW mode, indicating a gap flow bias away from it, but cylinder 2 is in the NW mode only in $3600 \leq t^* \leq 4200$. This implies that different cross sections across the span of one cylinder could possibly be biased, less biased, or unbiased at $L^* = 1.18$. Moreover, one cross section could experience a gap flow bias away from it (lower drag than the time mean) while the corresponding cross section on the other cylinder experiences a less biased (similar drag as the time-mean) gap flow.

At a much lower Reynolds number of $Re = 500-3000$, Sumner et al. (1999), using PIV, found an intermittent “nearly symmetric near-wake” behind two smooth cylinders placed side-by-side with $L^* = 1.125$. For high subcritical flow ($Re = 4.7-5.5 \times 10^4$), Alam and Zhou (2007) reported that the gap flow intermittently sweeps around the cylinder in the NW mode, forming a separation bubble at $L^* = 1.1$. There was no separation bubble at $L^* = 1.2$ and multi-stable gap flow with and without the bubble at $L^* = 1.13$. On comparing the pressure distributions in Fig. 17(a) and those presented in Alam et al. (2003) when a separation bubble exists, it is clear that the intermediate modes at $L^* \in \{1.18, 1.2\}$ in the current investigation are not caused by an intermittent separation bubble. Rather, the current intermediate modes are due to intermittent “nearly symmetric” flow behavior as reported by Sumner et al. (1999).

Figure 18 gives spectra of lift fluctuations in the time periods identified previously in Fig. 16. Unlike the spectra at $L^* = 1.5$ shown in Fig. 11(b), both modes contain a prominent frequency at $fD/U_\infty \sim 0.1$. This suggests that the frequencies in lift in the shedding of one cylinder also excite the other cylinder, consistent with the small gap between the two cylinders. The spectrum corresponding to the NW mode additionally has a relatively less prominent broadband plateau near $fD/U_\infty \approx 0.3-0.4$, suggesting a weak periodicity of the larger harmonic mode of vortex shedding.

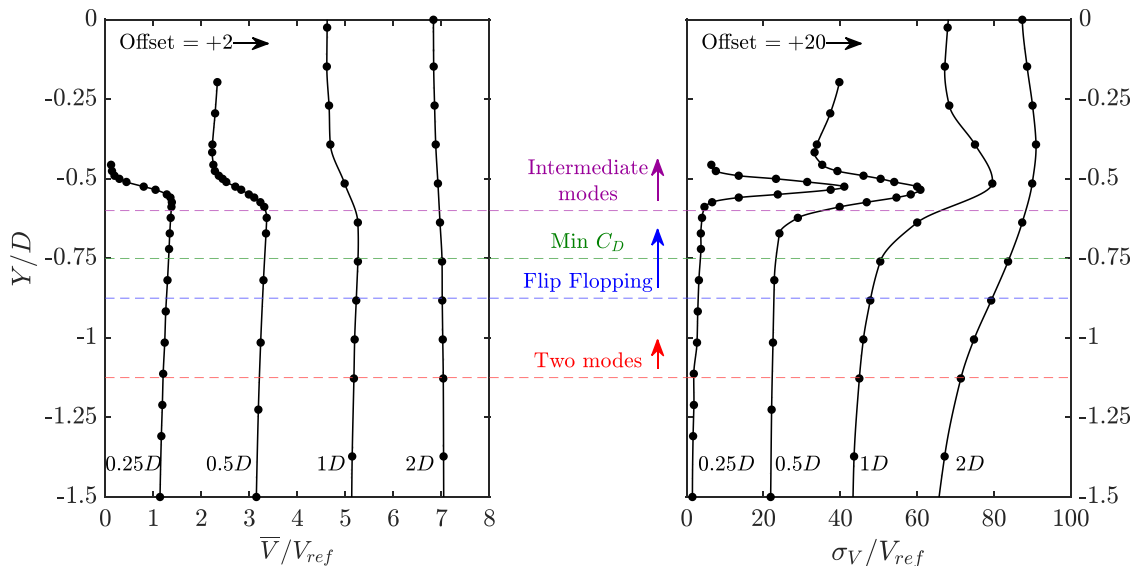


FIG. 19. Mean and fluctuating velocity distributions beside an isolated cylinder of the same surface roughness in an incoming Reynolds number of 2.9×10^5 . Text beside each curve indicates the downstream location from the center of cylinder. Successive curves are offset to increase legibility. Data from Pasam et al. (2023).

Interestingly, no prominent frequency peaks are found in the spectrum corresponding to $3100 \leq t^* \leq 5100$, where the gap flow is less biased. This implies a further reduction in the periodicity of lift fluctuations in the intermediate mode. The lift spectrum given in Fig. 6 contains a faint peak at $fD/U_\infty \sim 0.21$ unlike the spectra given in Fig. 18. The spectra shown in Fig. 6 are averages of spectra from all the tests done at a given pitch ratio and Reynolds numbers, and hence should be able to identify less prominent frequencies due to reduced noise.

G. Velocity profiles beside an isolated cylinder

Flow configurations found at various pitch ratios in the current system of two cylinders are expected to be strongly influenced by differences in the interaction of shear layers emanating from the two cylinders. Although the presence of a second cylinder alters the behavior of separated shear layers, the velocity distribution beside an isolated cylinder could still provide insight into understanding the wake flow behavior behind a two cylinder arrangement.

Figure 19 overlays the identified flow regimes over the mean and fluctuating velocity distributions beside an isolated cylinder at a Reynolds number of 2.9×10^5 . The boundaries of various flow regimes in the two cylinder arrangement are halved in the figure to account for shear layers from both the cylinders. For example, the minimum in C_D occurs at $L^* = 1.5$, this corresponds to shear layer interaction at $Y/D = 0.75$ from the center of either cylinder.

Notably, these measurements are done in the same facility, in flow over one of the two cylinders used in this investigation. A single-axis hot film anemometer was mounted on a traverse to obtain these distributions. This setup is explained in further detail in Pasam et al. (2023). The data presented here are reproduced from figure 21 in Pasam et al. (2023). Note that the velocity presented here is the in-plane velocity, i.e., $V = \sqrt{u^2 + v^2}$ where u , v , and w are the streamwise, cross-stream, and spanwise velocities, respectively. In addition, \bar{V} , V_{ref} , σ_V , and Y refer to the mean in-plane velocity, the reference velocity, the standard deviation of the in-plane velocity, and the cross-stream distance measured from the center of the cylinder, respectively.

As mentioned previously, “intermediate wake modes” are the modes with less bias or no bias in the wake and are less coherent in the spanwise direction compared to the traditional narrow-wake and wide-wake modes. These modes are seen for pitch ratios $L^* \leq 1.2$. It is clear from Fig. 19 that at these pitch ratios, the cylinders are close enough that the separated shear layers from the two cylinders interact closer than $0.5D$ downstream of the cylinder.

The boundaries of the remaining flow configurations are not as clearly pronounced in the velocity distributions. As the two cylinders are moved closer from large pitch ratios ($L^* = 6$), bias in the wake first occurs at $L^* \sim 2.25$, which appears to be a pitch ratio at which the shear layers from the two cylinders interact near $\sim 2D$ downstream from the center of the cylinder. Flip flopping between the two modes is seen for $L^* \leq 1.75$ which corresponds to shear layer interaction near $\sim 1D$ downstream of the cylinder.

The vortex formation length downstream of a smooth cylinder in postcritical flow is expected to be between 1 and 2 diameters downstream from the center (Ljungkrona et al., 1991). Hence, it comes as no surprise that the pitch ratio for the first appearance of the two modes is also the one where the separated shear layers from the two cylinders interact close to the vortex formation length. The pitch ratio

where the flip flopping between the two modes starts is the one where the shear layers interact upstream of the vortex formation length.

IV. CONCLUSIONS

Despite numerous previous investigations on the aerodynamics of two cylinders placed side by side, knowledge of *postcritical* flow over this geometrical arrangement remains limited. Even at subcritical Reynolds numbers, there are inconsistencies in some key aerodynamic parameters in the experimental studies. The current investigation reports on and interprets the flow behavior over two rough cylinders placed side by side in the postcritical regime and presents the measured aerodynamic coefficients and their dynamic behavior. Beyond that, together with the study of Pasam et al. (2024) on two rough *inline* cylinders, this study is directed toward providing a framework for understanding the more general arrangement of the two rough cylinders in the postcritical regime with both streamwise and cross-stream distance between them.

The relative surface roughness used in this investigation is $k_s/D = 1.9 \times 10^{-3}$ and each cylinder has an individual blockage of 5%. The Reynolds number of the incoming flow is maintained at $\sim 3 \times 10^5$ and the pitch ratio L^* varied from 1.18 to 6. While many aspects of the qualitative flow behavior in the postcritical regime are found to be analogous to those in subcritical Reynolds regime, there are some distinct differences, and quantitatively, there are considerable variations in the magnitudes of flow variables such as the drag and lift coefficients. The key findings of this investigation are as follows.

- (1) At a moderate spacing of $L^* = 6$, the mean drag coefficients of the two cylinders are the same to within experimental uncertainty. The drag coefficient, C_D , is 1.5% larger than that observed for an isolated cylinder *after adjusting for the same blockage as two isolated cylinders*. This is in agreement with the findings of Bearman and Wadcock (1973) for two smooth cylinders at $Re = 2.5 \times 10^4$. However, Alam et al. (2003) ($Re = 5.5 \times 10^4$) found agreement between the C_D of either cylinder at large pitch ratio and that of an isolated cylinder even without accounting for changes in the blockage.
- (2) In the biased regime, minima in the C_{D_s} of the cylinders experiencing the narrow-wake (NW) and wide-wake (WW) modes are observed near $L^* \sim 1.5$. The corresponding minimum in the averaged drag of the two cylinders, i.e., $\frac{1}{2}(C_{D_{NW}} + C_{D_{WW}})$, is $\sim 1.5\%$ greater than the blockage-adjusted C_D of an isolated cylinder. This minimum is not correlated to the differences in the location of boundary layer separation at different pitch ratios. Rather, it is caused due to extrema in the minimum pressure and base pressure on the circumferences of the cylinders. An increase in the gap (from $L^* = 1.18$) reduces the minimum pressure and base pressure on the inner halves of the cylinders until $L^* = 1.5$. Beyond $L^* = 1.5$, both the minimum pressure and base pressure increase with an increase in gap. This leads to the minimum in C_D at $L^* = 1.5$ for both cylinders (and modes).
- (3) The gap flow is predominantly biased and *flip flops* toward either cylinder in the region $1.18 \leq L^* \leq 1.75$. Within this L^* range, the mean drag of the two cylinders [i.e., $\frac{1}{2}(C_{D_{NW}} + C_{D_{WW}})$] is always larger than for an isolated cylinder *adjusted for 10% blockage*. For subcritical Reynolds numbers, Zdravkovich (1977) reported that the mean drag is always smaller, while Alam et al. (2003) reported that the mean drag is

smaller at certain pitch ratios than the mean drag on an isolated cylinder (without accounting for blockage). Along with the differences in measurement techniques, additional uncertainty associated with blockage corrections could be the reason behind this discrepancy.

- (4) Recent numerical simulations (Chen *et al.*, 2022; Zeng *et al.*, 2023) on two smooth cylinders placed side by side at low Reynolds numbers ($\mathcal{O}(10^3)$) revealed that the cylinder experiencing the larger drag (i.e., that with the NW mode) also experiences larger lift within the biased regime and outside the transitional pitch ratio range. In contrast, Alam *et al.* (2003) and Alam and Zhou (2007), through wind tunnel experiments on the same arrangement at $Re \sim \mathcal{O}(10^4)$, reported otherwise, i.e., that the (cylinder with the) NW mode has a lower lift coefficient than the WW mode irrespective of pitch ratio. In agreement with the numerical simulations, current wind tunnel investigations in the postcritical regime ($Re \sim \mathcal{O}(10^5)$) suggest that the NW mode also experiences larger lift for $1.33 \leq L^* \leq 1.75$, while the lift coefficients of the two modes are similar for $L^* \in \{1.18, 1.2\}$ and $L^* \in \{1.875, 2\}$. While these differences might be attributed to the differences in the Reynolds numbers of the investigations and/or the measurement techniques, an analysis of previous results on staggered cylinder arrangements from Price and Paidoussis (1984) and Sumner *et al.* (2005) suggests otherwise. Of note, the Reynolds number of Price and Paidoussis (1984) (6.4×10^4) is close to that of Alam *et al.* (2003) (5.5×10^4). Current results also indicate that this discrepancy is not due to the influence of the spanwise variation of the two modes on force measurements on the cylinder. Furthermore, this investigation found that the lift coefficients for the two modes, measured through the integration of pressures reported by Alam *et al.* (2003), do not agree with the corresponding lift coefficients measured through load cells [also reported by Alam *et al.* (2003)].
- (5) The variation of stagnation angles on the cylinders with pitch ratio in the current, and postcritical investigation are in good agreement with numerical simulations of low Reynolds number flows (Afgan *et al.*, 2011; Chen *et al.*, 2022; and Zeng *et al.*, 2023). This indicates that the influence of Reynolds number and surface roughness on flow behavior immediately upstream of the cylinders is minor, i.e., this aspect of the flow is geometry dominated. Surprisingly, these stagnation angles are also found to be in good agreement with the near wake deflection angles measured using PIV in Sumner *et al.* (1999) for $Re = 500\text{--}3000$, suggesting that the bias in the flow with respect to the line of symmetry is similar both upstream and downstream of the cylinders.
- (6) For all pitch ratios, the separation angles for both wake modes are similar on the outer halves of the two cylinders. In the inner half,
 - (i) The boundary layer on the cylinder in the NW mode separates later than in the WW mode for a given pitch ratio.
 - (ii) As the pitch ratio is increased from $L^* = 1.18$, the boundary layer on the cylinder experiencing the NW mode separates earlier.
 - (iii) The boundary layer on the cylinder with the WW mode separates at the similar location at all pitch ratios.

These trends are in agreement with those found in the numerical results from Afgan *et al.* (2011) for two smooth cylinders at the much lower sub-critical Reynolds number of 3900.

- (7) Intermediate modes with little bias in the gap region were previously found in low Reynolds number flow [at $L^* = 1.125$ for $Re \sim 3000$ in Sumner *et al.* (1999)] and for high subcritical flow [for $L^* \leq 1.13$ for $Re = 4.7 \times 10^4$ in Alam and Zhou (2007)]. The current investigation confirms their existence in the post-critical regime for $L^* \in \{1.18, 1.2\}$. While the modes in Sumner *et al.* (1999) are a result of intermittent nearly symmetric gap flow, those in Alam and Zhou (2007) are due to the intermittent formation of a separation bubble in the inner half of cylinder in the NW mode. Intermediate modes observed in the current postcritical flows appear similar to the former. In addition, current results suggest that intermediate modes reduce coherence in the spanwise direction, i.e., adjacent cross-sections of the cylinder could experience different biases in the gap flow. Over $1.33 \leq L^* \leq 2$, gap flow bias is the same at the two spanwise cross-sections measured at two diameters apart.
- (8) As the cylinders are moved closer from large pitch ratios, the first appearance of the “narrow-wake mode” and the “wide-wake mode” seems to be connected to the interaction between the shear layers emanating from the two cylinders just downstream of the vortex formation length. Flip flopping between the two modes is seen at pitch ratios where the shear layers interact prior to larger-scale wake vortex formation. The intermediate modes appear when the pitch ratio is such that the separated shear layers of the two cylinders interact immediately downstream of separation ($< 0.5D$ from the center of the cylinder).

ACKNOWLEDGMENTS

This research was supported by the Australian Government through the Australian Research Council’s Linkage Projects funding scheme (Grant No. LP180100234).

AUTHOR DECLARATIONS

Conflict of Interest

The authors have no conflicts to disclose.

Author Contributions

Anil Pasam: Conceptualization (equal); Data curation (equal); Formal analysis (equal); Investigation (equal); Methodology (equal); Validation (equal); Visualization (equal); Writing – original draft (equal). **Daniel Tudball Smith:** Conceptualization (equal); Methodology (equal); Project administration (equal); Resources (supporting); Supervision (supporting); Validation (supporting); Visualization (supporting); Writing – review & editing (supporting). **David Burton:** Conceptualization (equal); Funding acquisition (equal); Project administration (equal); Resources (lead); Supervision (lead); Validation (supporting); Visualization (supporting); Writing – review & editing (supporting). **Mark C. Thompson:** Conceptualization (equal); Funding acquisition (equal); Project administration (equal); Resources (equal); Supervision (equal); Validation (equal); Visualization (equal); Writing – review & editing (equal).

DATA AVAILABILITY

The data that support the findings of this study are available from the corresponding author upon reasonable request.

REFERENCES

- Achenbach, E., "Influence of surface roughness on the cross-flow around a circular cylinder," *J. Fluid Mech.* **46**, 321–335 (1971).
- Afgan, I., Kahil, Y., Benhamadouche, S., and Sagaut, P., "Large eddy simulation of the flow around single and two side-by-side cylinders at subcritical Reynolds numbers," *Phys. Fluids* **23**, 075101 (2011).
- Alam, M., Moriya, M., and Sakamoto, H., "Aerodynamic characteristics of two side-by-side circular cylinders and application of wavelet analysis on the switching phenomenon," *J. Fluids Struct.* **18**, 325–346 (2003).
- Alam, M. M. and Zhou, Y., "Flow around two side-by-side closely spaced circular cylinders," *J. Fluids Struct.* **23**, 799–805 (2007).
- Alam, M. M., Zhou, Y., and Wang, X. W., "The wake of two side-by-side square cylinders," *J. Fluid Mech.* **669**, 432–471 (2011).
- Allen, H. J. and Vincenti, W. G., "Wall interference in a two-dimensional-flow wind tunnel, with consideration for the effect of compressibility," NACA Tech. Rep., 1944; available at <https://ntrs.nasa.gov/citations/19930091861>.
- Batham, J. P., "Pressure distributions on circular cylinders at critical Reynolds numbers," *J. Fluid Mech.* **57**, 209–228 (1973).
- Bearman, P. W., "The effect of base bleed on the flow behind a two-dimensional model with a blunt trailing edge," *Aeronaut. Q.* **18**, 207–224 (1967).
- Bearman, P. W. and Wadcock, A. J., "The interaction between a pair of circular cylinders normal to a stream," *J. Fluid Mech.* **61**, 499–511 (1973).
- Bergh, H. and Tijdeman, H., "Theoretical and experimental results for the dynamic response of pressure measuring systems," Nationaal Lucht- en Ruimtevaartlaboratorium, 1965.
- Chen, W., Ji, C., Alam, M. M., and Yan, Y., "Three-dimensional flow past two stationary side-by-side circular cylinders," *Ocean Eng.* **244**, 110379 (2022).
- Güven, O., Farrell, C., and Patel, V. C., "Surface-roughness effects on the mean flow past circular cylinders," *J. Fluid Mech.* **98**, 673–701 (1980).
- Le Gal, P., Chauve, M. P., Lima, R., and Rezende, J., "Coupled wakes behind two circular cylinders," *Phys. Rev. A* **41**, 4566–4569 (1990).
- Ljungkrona, L., Norberg, C., and Sundén, B., "Free-stream turbulence and tube spacing effects on surface pressure fluctuations for two tubes in an in-line arrangement," *J. Fluids Struct.* **5**, 701–727 (1991).
- Nikurdase, J., "Laws of flow in rough pipes," NACA Technical Memorandum 1292 (1933).
- Norberg, C., "Fluctuating lift on a circular cylinder: Review and new measurements," *J. Fluids Struct.* **17**, 57–96 (2003).
- Pasam, A., Smith, D. T., Burton, D., and Thompson, M. C., "Flow over two inline rough cylinders in the postcritical regime," *Phys. Fluids* **36**, 095145 (2024).
- Pasam, A., Smith, D. T., Holmes, J. D., Burton, D., and Thompson, M. C., "The influence of surface roughness on postcritical flow over circular cylinders revisited," *J. Fluid Mech.* **975**, A36 (2023).
- Price, S. and Paidoussis, M., "The aerodynamic forces acting on groups of two and three circular cylinders when subject to a cross-flow," *J. Wind Eng. Ind. Aerodyn.* **17**, 329–347 (1984).
- Roshko, D., "Experiments on the flow past a circular cylinder at very high Reynolds number," *J. Fluid Mech.* **10**, 345–356 (1961).
- Schewe, G., "On the force fluctuations acting on a circular cylinder in crossflow from subcritical up to transcritical Reynolds numbers," *J. Fluid Mech.* **133**, 265–285 (1983).
- Speidel, L., "Einfluß der oberflächenrauigkeit auf die strömungsverluste in ebenen schaufelgittern," *Forsch. Ing.-Wes.* **20**, 129–140 (1954).
- Spivack, H. M., "Vortex frequency and flow pattern in the wake of two parallel cylinders at varied spacing normal to an air stream," *J. Aeronaut. Sci.* **13**, 289–301 (1946).
- Sumner, D., "Two circular cylinders in cross-flow: A review," *J. Fluids Struct.* **26**, 849–899 (2010).
- Sumner, D., Richards, M., and Akosile, O., "Two staggered circular cylinders of equal diameter in cross-flow," *J. Fluids Struct.* **20**, 255–276 (2005).
- Sumner, D., Wong, S. S. T., Price, S. J., and Paidoussis, M. P., "Fluid behaviour of side-by-side circular cylinders in steady cross-flow," *J. Fluids Struct.* **13**, 309–338 (1999).
- Sun, T., Gu, Z., He, D., and Zhang, L., "Fluctuating pressure on two circular cylinders at high Reynolds numbers," *J. Wind Eng. Ind. Aerodyn.* **41**, 577–588 (1992).
- Szechenyi, E., "Supercritical Reynolds number simulation for two-dimensional flow over circular cylinders," *J. Fluid Mech.* **70**, 529–542 (1975).
- Williamson, C. H. K., "Evolution of a single wake behind a pair of bluff bodies," *J. Fluid Mech.* **159**, 1 (1985).
- Xu, S. J., Zhou, Y., and So, R. M. C., "Reynolds number effects on the flow structure behind two side-by-side cylinders," *Phys. Fluids* **15**, 1214–1219 (2003).
- Zdravkovich, M. M., "Review of flow interference between two circular cylinders in various arrangements," *J. Fluids Eng.* **99**, 618–633 (1977).
- Zeng, C., Qiu, F., Zhou, J., Hu, Y., and Wang, L., "Large eddy simulation of flow around two side-by-side circular cylinders at Reynolds number 3900," *Phys. Fluids* **35**, 035102 (2023).
- Zhou, Y. and Alam, M. M., "Wake of two interacting circular cylinders: A review," *Int. J. Heat Fluid Flow* **62**, 510–537 (2016).
- Zhou, Y., Zhang, H. J., and Yiu, M. W., "The turbulent wake of two side-by-side circular cylinders," *J. Fluid Mech.* **458**, 303–332 (2002).